OFFICE OF CIVILIAN RADIOACTIVE WASTE MANAGEMENT

CALCULATION COVER SHEET

1. QA: QA
Page: 1 Of: 68

2. Calculation Title

Precipitates/Salts Model Sensitivity Calculations

3. Document Identifier (including Revision Number)

CAL-EBS-PA-000010 REV 00

4. Total Attachments	5. Attachment Numbers -- Number of pages in each
0	N/A

	Print Name	Signature	Date
6. Originator	Paul Mariner	Randolph L Scheer for	20 Dec 01
7. Checker	Darren Jolley	Darren Jolley	12/20/01
8. Lead	James Nowak	Randolph L Scheer for	20 Dec 01

9. Remarks

This calculation uses the High Relative Humidity salts model developed in *In-Drift Precipitates/Salts Analysis* (ANL-EBS-MD-000045 Rev. 00 ICN 03) to predict evaporative evolution of a wide range of predicted and observed Yucca Mountain waters.

Revision History

10. Revision No.	11. Description of Revision
00	Initial issue.

CONTENTS

Page

FIGURES

Page

TABLES

Page

ACRONYMS AND ABBREVIATIONS

ACC	accession number
AMR	Analysis/Model Report
BSC	Bechtel SAIC Company
C_i	concentration of component *i* in the incoming seepage
C/C_o	concentration factor
CRWMS M&O	Civilian Radioactive Waste Management Services Management and Operations
DIRS	Data Input Reference System
DTN	Data Tracking Number
EBS	Engineered Barrier System
f_{CO2}	carbon dioxide (CO_2) fugacity
HRH	high relative humidity
I	ionic strength
ISa	ionic strength approximation (Equation 1)
LRH	low relative humidity
PT4	data0.pt4, a thermodynamic database developed in this AMR for EQ3/6
PT5v2	data0.pt5, a revision of PT4, version 2
SSPA	Supplemental Science and Performance Analyses
THC	thermal hydrological-chemical
TIC	Technical Information Center
TPO	technical product output
TSPA	Total System Performance Assessment
TSw	Topopah Spring welded hydrogeologic unit
TWP	Technical Work Plan

1. PURPOSE

The objective and scope of this calculation is to assist Performance Assessment Operations and the Engineered Barrier System (EBS) Department in modeling the geochemical effects of evaporation on potential seepage waters within a potential repository drift. This work is developed and documented using procedure AP-3.12Q, *Calculations*, in support of *Technical Work Plan For Engineered Barrier System Department Modeling and Testing FY 02 Work Activities* (BSC 2001a).

The specific objective of this calculation is to examine the sensitivity and uncertainties of the Precipitates/Salts model. The Precipitates/Salts model is documented in an Analysis/Model Report (AMR), *In-Drift Precipitates/Salts Analysis* (BSC 2001b). The calculation in the current document examines the effects of starting water composition, mineral suppressions, and the fugacity of carbon dioxide (CO_2) on the chemical evolution of water in the drift.

2. METHOD

The High Relative Humidity (HRH) submodel of the Precipitates/Salts model was used to perform the calculations in this document. This submodel, explained in detail in *In-Drift Precipitates/Salts Analysis* (BSC 2001b, Section 6.4.2), is summarized in Section 4, as are the methods of calculation. Any deviations from these methods are explained in detail in Sections 3 and 5. The control of electronic management of data was accomplished in accordance with methods specified in the Technical Work Plan (TWP) (BSC 2001a).

3. ASSUMPTIONS

The model assumptions for this calculation are identical to HRH submodel assumptions described in Section 5 of *In-Drift Precipitates/Salts Analysis* (BSC 2001b) and Section 3 of *Precipitates/Salts Model Results for THC Abstraction* (CRWMS M&O 2001).

Assumptions were also made for the first seven input data sets listed in Table 1 (i.e., waters #1 through #7). These input assumptions are described in detail in the following subsections.

3.1 IN SITU AVERAGE J-13 WELL WATER

The mean pH and mean concentrations of major ions in average J-13 well water have been qualified based on Harrar et al. (1990) and documented in DTN: MO0006J13WTRCM.000. Although these data are qualified, the pH value in the qualified reference does not represent the average value for J-13 water in situ (Harrar et al 1990, p. 4-9). Therefore, based on additional information from Harrar et al. (1990), five assumptions are made as described below to adjust the J-13 water composition for in situ aquifer conditions. These five assumptions are justified because 1) they are based on the same report (Harrar et al. 1990) used to qualify the average J-13 well water measurements, and/or 2) they correct the data set for electrical balance. These assumptions are used in Section 6.1.2.1.

Assumption 3.1.1. The pH is set at the approximate mean *field* measurement of 7.0 (Harrar et al. 1990 p. 4-9).

Rationale: This assumption is justified because many of the pH values averaged in the Harrar et al. (1990) report are lab measurements (Harrar et al 1990, p. 4-9), which are typically higher than field measurements, likely due to loss of dissolved CO_2 (Harrar et al 1990, p. 4-9). As shown in the results (DTN: MO0112MWDHRH10.025, file: J13.3O), a pH of 7.0 for this data set implies an equilibrium in situ log fugacity of CO_2 around -1.86. This fugacity is reasonable for ground water in aquifers containing calcite (Drever 1988, p. 67) and further justifies the in situ pH 7.0 value. No further confirmation is required for this assumption.

Assumption 3.1.2. The mean measured alkalinity from DTN: MO0006J13WTRCM.000 is entered as 128.9 "free mg/L" as bicarbonate (HCO_3^-).

Rationale: This treatment of the alkalinity measurement fixes the HCO_3^- species concentration at 128.9 mg/L and assumes that all of the mean measured alkalinity is from the HCO_3^- species. This assumption is justified by the results, which indicate that the HCO_3^- species accounts for more than 99 percent of the alkalinity at pH 7.0 (DTN: MO0112MWDHRH10.025, file: J13.3O). No further confirmation is required for this assumption.

This treatment of alkalinity allows EQ3NR to determine how much H_2CO_3 (aq) to add to the solution to bring it into equilibrium with the pH of 7.0. This is important because the H_2CO_3 (aq) concentration is not included in an alkalinity measurement. For water with a pH in the neutral or acid range, H_2CO_3 (aq) accounts for a considerable portion of the total dissolved carbonate (Drever 1988, p. 55).

Assumption 3.1.3. The water is charge balanced by allowing EQ3NR to adjust the HCO_3^- concentration as needed.

Rationale: According to the results (DTN: MO0112MWDHRH10.025, file: J13.3O), charge balancing with HCO_3^- causes the equilibrated alkalinity to be about one percent below the mean measured alkalinity. This assumption is justified because the relative standard deviation of the alkalinity data in the Harrar report is 6.7 percent (DTN: MO0006J13WTRCM.000). No further confirmation is required for this assumption.

Assumption 3.1.4. Redox is set by setting the log fugacity of O_2 (g) to -0.818, which yields an O_2 (aq) concentration of 5.6 mg/L (DTN: MO0112MWDHRH10.025, file: J13.3O).

Rationale: This value is justified and confirmed because Harrar et al. (1990, p. 4-9) reports values of 5.5 to 5.7 mg/L for O_2 (aq). The actual log fugacity of O_2 (g) for this water is not important in the current document, however, because no redox reactions are important in the calculations. It is only included in the input because EQ3NR requires a redox parameter value. No further confirmation is required for this assumption.

Assumption 3.1.5. Temperature is set at the downhole temperature of 31ºC reported in Harrar et al. (1990, p. 4-9).

Rationale: This temperature is justified because it is reported in the same report (Harrar et al. 1990) used to qualify the average J-13 well water measurements. No further confirmation is required for this assumption.

3.2 NITRATE CONCENTRATIONS

Nitrate was added to three of the waters listed in Table 1, the Topopah Spring tuff pore water (water #2) and THC abstraction waters (waters #6 and #7). Nitrate concentrations are not reported for these waters. The concentration of nitrate added was determined based on an assumed nitrate to chloride molar ratio. The primary reason nitrate was added was to track the concentration factor during evaporation because nitrate behaves conservatively in the calculations.

Assumption 3.2.1. The molar ratio of nitrate to chloride for pore water from the Topopah Spring welded hydrogeologic unit (TSw) and for abstracted THC model seepage water is assumed to be 0.1. This assumption is used in Sections 6.1.2.2, 6.1.2.6, and 6.1.2.7.

Rationale: This molar ratio is justified based on a rounded average of the molar ratios in the four TSw pore water samples listed in Table 6 of CRWMS M&O (2000a, pp. I-17 and I-19). No further confirmation is required for this assumption.

3.3 PERCHED WATER COMPOSITION

Assumption 3.3.1. Because perched water is a subset of ambient fluids that could seep into drifts and contact waste packages, a potential fluid composition representing perched water has been selected for use in the sensitivity calculations presented below. The assumed representative perched water composition is identical to a perched water sample collected on 8/3/1993 from borehole USW UZ-14 within the Topopah Spring welded unit. This composition is documented in Table 8 of CRWMS M&O (2000a, p. I-22). This assumption is used in Section 6.1.2.3.

Rationale: The assumed representative perched water composition is corroborated by other perched water sample measurements listed in Table 8 of CRWMS M&O (2000a, p. I-22). This composition has been used in previous sensitivity studies using previous versions of the Precipitates/Salts model (Mariner 2001). The use of this assumed input allows for direct comparison to previous sensitivity calculations. Because results for sensitivity studies are not generally used as direct input into TSPA models, this composition is sufficient to evaluate the representative potential effects. Therefore, this assumption is justified and requires no further confirmation.

3.4 SINGLE HEATER TEST WATER COMPOSITION

Assumption 3.4.1. Because Single Heater Test waters are a potential subset of thermally perturbed waters that could seep into drifts and contact waste packages, a potential fluid composition representing Single Heater Test water has been selected for use in the sensitivity calculations presented below. The assumed representative composition of Single Heater Test water is a Single Heater Test water sample collected on 2/3/1997 from borehole 16, Suite 2.

This composition is documented in Table 5-19 of CRWMS M&O (1997, p. 5-49). This assumption is used in Section 6.1.2.4.

Rationale: The assumed representative Single Heater Test water composition is corroborated by Suite 1 Single Heater Test water composition measurements (CRWMS M&O 1997, p. 5-49) and other Single Heater Test water compositions reported in DTN: LL970409604244.030. This composition has been used in previous sensitivity studies using previous versions of the Precipitates/Salts model (Mariner 2001). The use of this assumed input allows for direct comparison to previous sensitivity calculations. Because results for sensitivity studies are not generally used as direct input into TSPA models, this composition is sufficient to evaluate the representative potential effects. Therefore, this assumption is justified and requires no further confirmation.

3.5 DRIFT-SCALE HEATER TEST WATER COMPOSITION

Assumption 3.5.1. Because Drift-Scale Heater Test waters are a potential subset of thermally perturbed waters that could seep into drifts and contact waste packages, a potential fluid composition representing Drift-Scale Heater Test water has been selected for use in the sensitivity calculations presented below. The assumed representative composition of Drift-Scale Heater Test water is a Drift-Scale Heater Test water sample collected on 1/26/1999 from borehole 60-3. This composition is documented in DTN: LL990702804244.100. This assumption is used in Section 6.1.2.5.

Rationale: This water composition is corroborated by other Drift-Scale Heater Test water compositions reported in DTN: LL990702804244.100 and has been used in previous sensitivity studies using previous versions of the Precipitates/Salts model (Mariner 2001). The use of this assumed input allows for direct comparison to previous sensitivity calculations. Because results for sensitivity studies are not generally used as direct input into TSPA models, this composition is sufficient to evaluate the representative potential effects. Therefore, this assumption is justified and requires no further confirmation.

4. USE OF COMPUTER SOFTWARE AND MODELS

4.1 MODELS

The Precipitates/Salts model, developed and validated in *In-Drift Precipitates/Salts Analysis* (BSC 2001b), was used to perform the calculations in this document. The model incorporates two submodels, the Low Relative Humidity (LRH) model and the High Relative Humidity (HRH) model. Only the HRH model is used in this calculation. The HRH model is simulated using the geochemical code EQ3/6 version 7.2b.

Use of the Precipitates/Salts model in this calculation is justified because the model was specifically designed to perform these calculations (BSC 2001b).

4.2 SOFTWARE

All computer calculations were performed on a Hewlett Packard Pavilion 7410P, an IBM-compatible personal computer, serial number US72352516. This computer uses a Microsoft Windows 95 operating system and is located in Colorado Springs, Colorado.

The evaporation calculations were performed using the code EQ3/6 v7.2b [CSCI: URCL-MA-110662, Wolery 1992a and 1992b, Wolery and Daveler 1992, CRWMS M&O 1998a] with the solid-centered flow-through addendum [EQ6 V7.2bLV, STN: 10075-7.2bLV-00, CRWMS M&O 1999a and 1999b]. These software were obtained from Configuration Management. They were appropriate for the application and were used only within the range of validation in accordance with AP-SI.1Q *Software Management* and the Precipitates/Salts AMR (BSC 2001b). The Precipitates/Salts AMR restricts the use of these codes to a water activity of about 0.85 and higher.

Microsoft Excel 97 SR-2, a commercially-available spreadsheet software package, was used to chart data and to calculate the ionic strength approximation (*ISa*) and concentration factor (C/C_o). Spreadsheet calculations were validated by hand calculations using the equations presented in Section 5.2, and charts were validated by visual inspection. These actions confirm that the spreadsheet application provided correct results. No macros or software routines were developed for, or used by, this software, and consequently it is an exempt software application in accordance with Section 2.1 of AP-SI.1Q.

5. CALCULATION

Section 5.1 describes the input to the calculations while Section 5.2 describes the calculations performed.

5.1 INPUT

The calculations required the following types of input: 1) thermodynamic constants for potentially important ground-water constituents, and 2) values for model input variables.

5.1.1 Thermodynamic Database

The thermodynamic database used in each evaporation calculation was the PT5v2 Pitzer thermodynamic database (DTN: MO0110SPAPT245.017). This database is developed in the Precipitates/Salts AMR (BSC 2001b).

5.1.2 Input Variables

The input variables for the simulations include temperature, pH, fugacity of CO_2, redox potential, and initial concentrations of the aqueous components. Table 1 lists the sources of the acquired input data used in the EQ3/6 input files in this calculation.

Not all waters identified in Table 1 have a complete set of values for input variables. The redox potential is only specified for a few of the waters. However, no redox reactions were simulated, so the values entered for redox potential did not affect the results presented. Waters #1 through #5 were evaporated at 96°C and were evaporated at three different values for CO_2 fugacity: 10^{-1}, 10^{-3}, and 10^{-6}. Temperature and CO_2 fugacity values used for waters #6 through #9 correspond to the source input values.

The following minerals were suppressed in each of the model runs: K-feldspar, maximum microcline, dolomite, magnesite, quartz, albite, tridymite, diaspore, enstatite, wollastonite, anorthite, talc, chrysotile, and anhydrite. These minerals were suppressed because their formation is likely too slow at the temperatures and pressures modeled (BSC 2001b, Table 16; Klein and Hurlbut 1999) or their precipitation would be inconsistent with the minerals predicted to precipitate in the thermal hydrological-chemical (THC) model. An example of the latter is that gypsum is used in the THC model instead of anhydrite. Several of the suppressed minerals never became supersaturated in the calculations (Section 6); they were included as suppressed minerals in the input files simply to prevent rerunning calculations in the event an undesired mineral became supersaturated.

Table 1. References for Data Used in EQ3/6 Input Files

Water	Description of Data Used	Reference
1	Recommended mean values of major constituents in J-13 well water	DTN: MO0006J13WTRCM.000
	Parameter adjustments to represent average in situ J-13 well water	Assumptions 3.1.1 through 3.1.5
2	Pore water composition and CO_2 partial pressure input to REV 01 thermal hydrological-chemical (THC) simulations	DTN: LB0101DSTTHCR1.001
	Nitrate to chloride molar ratio	Assumption 3.2.1
3	Chemical composition of perched water sample collected from borehole USW UZ-14 within the Topopah Spring welded unit on 8/3/1993	Assumption 3.3.1
4	Chemical composition of Single Heater Test water sample collected from borehole 16, Suite 2	Assumption 3.4.1
5	Chemical analysis of Drift-Scale Heater Test water sample from borehole 60-3 on 1/26/1999	Assumption 3.5.1
6	Abstraction of THC REV 00 model chemical boundary conditions for abstraction periods 2, 3, and 4	DTN: MO9912SPAPAI29.002
	Nitrate to chloride molar ratio	Assumption 3.2.1
7 [a]	Abstraction of the REV 01 THC model results for seepage at the crown of the drift in the Tptpmn lithology	DTN: MO0112MWDTHC12.024 Files: mc$.6o [b]
	Nitrate to chloride molar ratio	Assumption 3.2.1
8	Cement grout leachate predicted to result from contacting cement with water #7	DTN: MO0111SPATHC14.040 Files: tb2??cm.6o [c]
9	Cement grout leachate predicted to result from contacting cement with water from the REV 01 THC model abstraction at the crown of the drift of the high temperature and high carbon dioxide partial pressure case in the Tptpll lithology, initialized using water composition of UZ-14 perched water	DTN: MO0111SPATHC14.040 Files: tb14??cm.6o [c]

[a] The EQ3/6 calculations performed for water #7 are documented in *Precipitates/Salts Model Calculations for Various Drift Temperature Environments* (BSC 2001c). DTN: MO0112MWDTHC12.024 includes EQ3/6 output files. These data are included in this document for comparison purposes.

[b] $ is a wildcard for the different abstraction time periods described in Table 3.

[c] ?? is a wildcard for pc, bc, cd, xd, ta, and am, corresponding respectively to time periods 1, 2, 3, 4, 5, and 6 in Table 3.

5.2 CALCULATIONS

Each evaporation calculation was performed using EQ3/6 according to the procedures described in Section 6.4.2.1 of the Precipitates/Salts AMR (BSC 2001b). Water was evaporated by declaring it a "special reactant" with a rate constant of -1.0. The maximum reaction progress was iteratively adjusted to achieve a final water activity of 0.85. Before each run, the water composition was electrically balanced by allowing EQ3/6 to adjust the bicarbonate, Na, Cl, or other major ion concentration, depending on which ion's concentration would be changed the least to achieve electrical balance.

Model predictions were exported to text files using the EQ3/6 postprocessor (PP.EXE) included in the EQ6 software package. These text files were imported into Excel worksheets where the ionic strength approximation (*ISa*) and concentration factor (C/C_o) could be calculated and the results plotted. C/C_o was calculated by dividing the total nitrate concentration by the initial nitrate concentration. Nitrate does not precipitate in the high relative humidity range modeled in these calculations.

The ionic strength approximation (*ISa*) parameter of the Precipitates/Salts model is not the true ionic strength. Instead, it is an approximation of the true ionic strength (*I*) according to the following equation:

$$ISa = C_{Na} + C_K + 4(C_{Ca} + C_{Mg}) \quad \text{(Eq. 1)}$$

where C_i is the molality of component *i*, and *i* represents sodium (Na), potassium (K), calcium (Ca), or magnesium (Mg). This approximation is included in the results because it is identical to the approximation used by the Precipitates/Salts model (BSC 2001b, Section 6.3.2) and colloids model (CRWMS M&O 1998b, Section 4.4.3.3.1).

6. RESULTS

In this section, the results of the sensitivity calculations are presented. They focus on the sensitivity of evaporative evolution to the following input parameters: (1) starting water composition, (2) mineral suppressions, and (3) CO_2 fugacity. These sensitivity calculations are presented in Sections 6.1, 6.2, and 6.3, respectively. Uncertainty and limitations are addressed in Section 6.4.

6.1 EFFECTS OF STARTING WATER COMPOSITION ON EVAPORATIVE EVOLUTION

An important uncertainty in the Precipitates/Salts model calculations is the sensitivity of the starting water composition on the evaporative chemical evolution of water in the drift. The REV 00 TSPA model makes the assumption that nitrate salts will set the lower limit on the relative humidity at which liquid water is stable within the drift (CRWMS M&O 2000b, Appendix F). To investigate the uncertainty in the different types of brines that might develop from evaporation, a set of sensitivity calculations was performed. The results show that the chemical composition of the remaining evaporated solution can be highly sensitive to the starting water composition. Furthermore, they suggest that basing the relative humidity threshold assumption on the properties of a sodium/potassium nitrate salt solution may not be appropriate in some instances. These results illustrate the importance of chemical divides encountered during evaporation.

6.1.1 The Chemical Divide

Evaporation of water is the net transfer of water molecules from liquid to vapor. As water evaporates from an aqueous solution, each solute concentrates until it becomes supersaturated with respect to a mineral phase and thereafter precipitates. If the mineral phase is a binary salt and the concentrations of the two reactants (multiplied by their stoichiometric coefficients) are not equal, then the reactant having the lower relative concentration (multiplied by its stoichiometric coefficient) will become depleted in solution while the other reactant will continue to concentrate (Eugster and Hardie 1978, pp. 243-247; Eugster and Jones 1979, pp. 614-629). This mechanism is known as a chemical divide (Drever 1988, pp. 235-236). A chemical divide establishes which reactant concentrations are predominantly controlled by the solubility of a precipitating phase (i.e., those that become depleted in solution) and which reactant concentrations are only partially controlled by a precipitating phase (i.e., those that continue to concentrate in solution despite partial precipitation).

A chemical divide is demonstrated in the following example. If, as water evaporates, halite (NaCl) reaches saturation and begins to precipitate and the Na:Cl molar ratio is greater than one, then Cl will become depleted in solution while excess Na will continue to concentrate. Inversely, if the ratio is less than one, then Na will become depleted while excess Cl will continue to concentrate. This mechanism implies that a small difference in the original Na:Cl ratio can determine whether a Na or Cl brine develops beyond the halite chemical divide.

Chemical divides are useful in explaining the chemical evolution of natural saline waters. The earliest example of this concerned the evaporative evolution of Sierra Nevada spring water

(Garrels and Mackenzie 1967). Upon evaporation, the first chemical divide encountered was the calcite chemical divide. Calcite precipitation is an important evolutionary step because the relative concentrations of Ca and carbonate (CO_3) determine whether the evaporating water becomes carbonate-poor or carbonate-rich (Eugster and Hardie 1978, pp. 244). In this case, there was excess CO_3 so the water became carbonate-rich and Ca was depleted. Next, precipitation of sepiolite depleted Mg. Continued evaporation resulted in a sodium carbonate brine with a pH near 10, which is common for natural saline lakes in the western United States (Eugster and Hardie 1978, p. 240). In the late stage of evaporation, the highly soluble components precipitate. In carbonate-rich brines, these salts include, but are not limited to, Na, Cl, SO_4, CO_3, and SiO_2 (Eugster and Hardie 1978, p. 244).

Evaporation of simulated J-13 well water produces an alkaline sodium carbonate brine (Rosenberg et al. 1999a). This is similar to the brine predicted for the evaporation of Sierra Nevada spring water (Garrels and Mackenzie 1967). Calcite and aragonite, both having a molecular formula of $CaCO_3$, are observed to precipitate in laboratory J-13 evaporation experiments (Rosenberg et al. 1999a). Because carbonate alkalinity exceeds the Ca concentration in the starting water composition, Ca becomes depleted as $CaCO_3$ precipitates.

Evaporation of simulated Topopah Spring tuff pore water gives the opposite result (Rosenberg et al. 1999b). This water has excess Ca relative to carbonate alkalinity and results in depletion of CO_3 and concentration of excess Ca. It results in a decrease in pH below 7 as the water continues to evaporate.

These two sets of results show that the evolution of waters at Yucca Mountain due to evaporative processes can be highly sensitive to the starting water composition. Section 6.1.2 presents evaporation predictions for several waters observed or predicted to occur at Yucca Mountain.

6.1.2 Evaporative Evolution of Observed or Predicted Yucca Mountain Waters

Evaporation calculations were performed for nine waters observed at Yucca Mountain or predicted to potentially occur in the drift. These waters, presented as waters #1 through #9 in Table 1, include the following (described and referenced in Section 5.1.2):

1. in situ J-13 ground water (i.e., average J-13 well water from Harrar et al. (1990) corrected for CO_2 degassing),
2. Topopah Spring tuff pore water,
3. water perched on top of the Calico Hills formation at the base of the Topopah Spring tuff,
4. water collected from the Single Heater Test,
5. water collected from the Drift-Scale Heater Test,
6. water predicted by the REV 00 THC model to seep into the crown of the drift,
7. water predicted by the REV 01 THC model to seep into the crown of the drift,
8. water predicted to result from reaction of cement with water #7, and
9. water predicted to result from reaction of cement with water from the REV 01 THC model abstraction of the high temperature and high CO_2 partial pressure case, initialized using water composition of UZ-14 perched water.

Figures 1 through 72 show the predicted evaporative evolution of these waters. A cross-reference for the outputs is presented in Table 2. Waters #6 through #9 are divided into abstraction periods. To simplify comparisons and identification of results, these periods are numbered in this document as described in Table 3. The results are summarized in Section 6.1.3.

Table 2. Output Files and Figures Cross-Reference

Water	Output Figures	EQ6 Output File	Output DTN
1	Figure 1 & Figure 2	J13-1.6O	MO0112MWDHRH10.025
	Figure 3 & Figure 4	J13-3.6O	MO0112MWDHRH10.025
	Figure 5 & Figure 6	J13-6.6O	MO0112MWDHRH10.025
2	Figure 7 & Figure 8	TSW-1.6O	MO0112MWDHRH10.025
	Figure 9 & Figure 10	TSW-3.6O	MO0112MWDHRH10.025
	Figure 11 & Figure 12	TSW-6.6O	MO0112MWDHRH10.025
3	Figure 13 & Figure 14	PERCH-1.6O	MO0112MWDHRH10.026
	Figure 15 & Figure 16	PERCH-3.6O	MO0112MWDHRH10.026
	Figure 17 & Figure 18	PERCH-6.6O	MO0112MWDHRH10.026
4	Figure 19 & Figure 20	SHT-1.6O	MO0112MWDHRH10.026
	Figure 21 & Figure 22	SHT-3.6O	MO0112MWDHRH10.026
	Figure 23 & Figure 24	SHT-6.6O	MO0112MWDHRH10.026
5	Figure 25 & Figure 26	DST-1.6O	MO0112MWDHRH10.026
	Figure 27 & Figure 28	DST-3.6O	MO0112MWDHRH10.026
	Figure 29 & Figure 30	DST-6.6O	MO0112MWDHRH10.026
6	Figure 31 & Figure 32	ABS2.6O	MO0112MWDHRH10.025
	Figure 33 & Figure 34	ABS3.6O	MO0112MWDHRH10.025
	Figure 35 & Figure 36	ABS4.6O	MO0112MWDHRH10.025
7	Figure 37 & Figure 38	MC1.6O	MO0112MWDTHC12.024
	Figure 39 & Figure 40	MC2.6O	MO0112MWDTHC12.024
	Figure 41 & Figure 42	MC3.6O	MO0112MWDTHC12.024
	Figure 43 & Figure 44	MC4.6O	MO0112MWDTHC12.024
	Figure 45 & Figure 46	MC5.6O	MO0112MWDTHC12.024
	Figure 47 & Figure 48	MC6.6O [a]	MO0112MWDTHC12.024
8	Figure 49 & Figure 50	MCC1.6O	MO0112MWDHRH10.025
	Figure 51 & Figure 52	MCC2.6O	MO0112MWDHRH10.025
	Figure 53 & Figure 54	MCC3.6O	MO0112MWDHRH10.025
	Figure 55 & Figure 56	MCC4.6O	MO0112MWDHRH10.025
	Figure 57 & Figure 58	MCC5.6O	MO0112MWDHRH10.025
	Figure 59 & Figure 60	MCC6.6O	MO0112MWDHRH10.025
9	Figure 61 & Figure 62	HHCPC1.6O	MO0112MWDHRH10.025
	Figure 63 & Figure 64	HHCPC2.6O	MO0112MWDHRH10.025
	Figure 65 & Figure 66	HHCPC3.6O	MO0112MWDHRH10.025
	Figure 67 & Figure 68	HHCPC4.6O	MO0112MWDHRH10.025
	Figure 69 & Figure 70	HHCPC5.6O	MO0112MWDHRH10.025
	Figure 71 & Figure 72	HHCPC6.6O	MO0112MWDHRH10.025

[a] The input for this run is mistakenly from the invert instead of the crown. However, the differences in these inputs are small (BSC 2001d, Tables 4 and 5) and easily within the range of uncertainty in the derived abstracted input values (BSC 2001d, Section 6.3). The crown seepage values are within 2 percent of the invert values, except for Mg, which is nearly 10 percent higher in the invert seepage (BSC 2001d, Tables 4 and 5).

Table 3. Key to Abstraction Time Periods Cited in This Report

Abstraction Time Period	[%]Water #6	[#]Waters #7 and #8	[#]Water #9
1	not simulated	0-50 years	0-50 years
2	50-1,000 years	51-1,200 years	51-1,500 years
3	1,000-2,000 years	1,201-2,000 years	1,501-4,000 years
4	2,000-100,000 years	2,001-20,000 years	4,001-25,000 years
5	not defined	20,001-100,000 years	25,001-100,000 years
6	not defined	100,001-1,000,000 years	100,001-1,000,000 years

[%]DTN: MO9912SPAPAI29.002, [#]MO0110SPAEBS13.038

6.1.2.1 In Situ J-13 Well Water (Water #1)

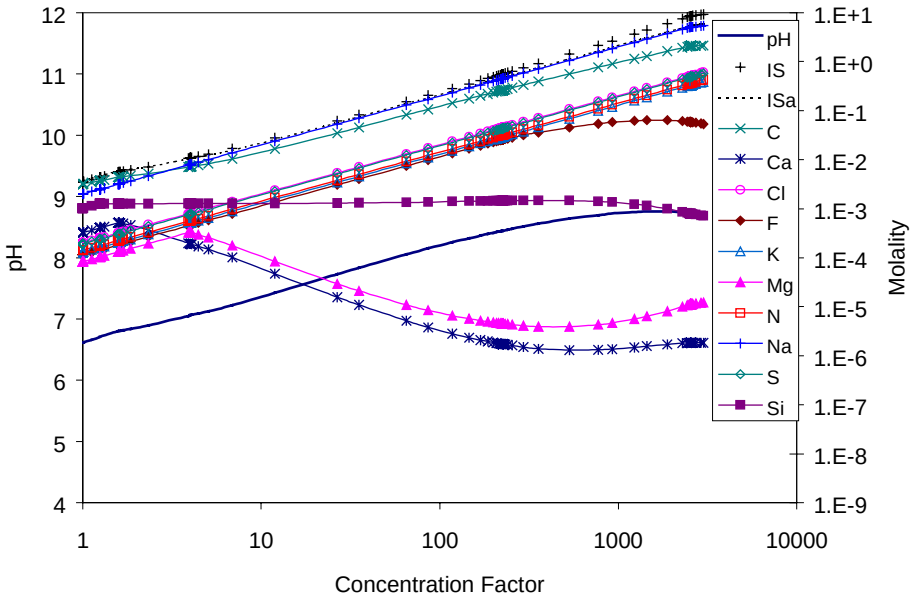

DTN: MO0112MWDHRH10.025

Figure 1. Aqueous Evaporative Evolution of In Situ J-13 Well Water at f_{CO2} of 10^{-1}

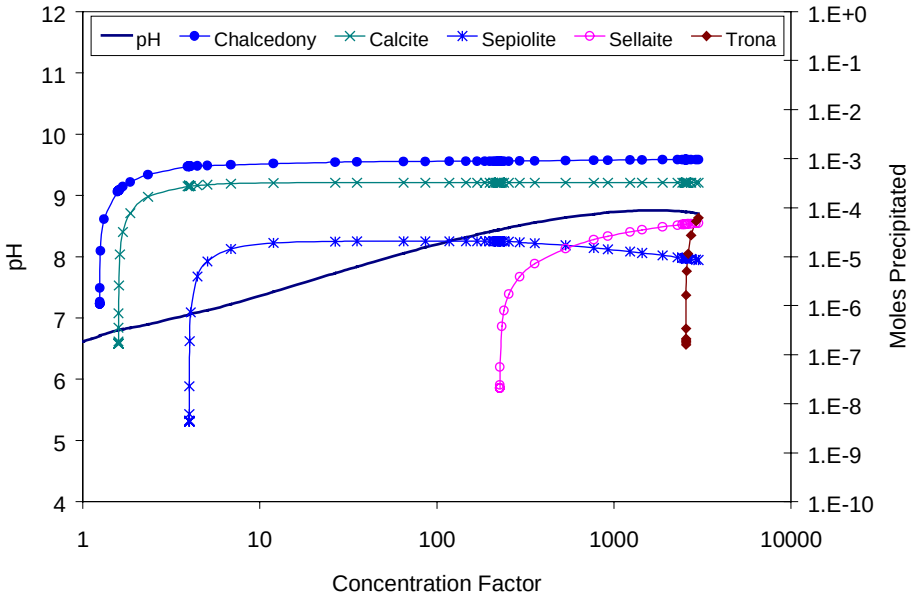

DTN: MO0112MWDHRH10.025

Figure 2. Mineral Evaporative Evolution of In Situ J-13 Well Water at f_{CO2} of 10^{-1}

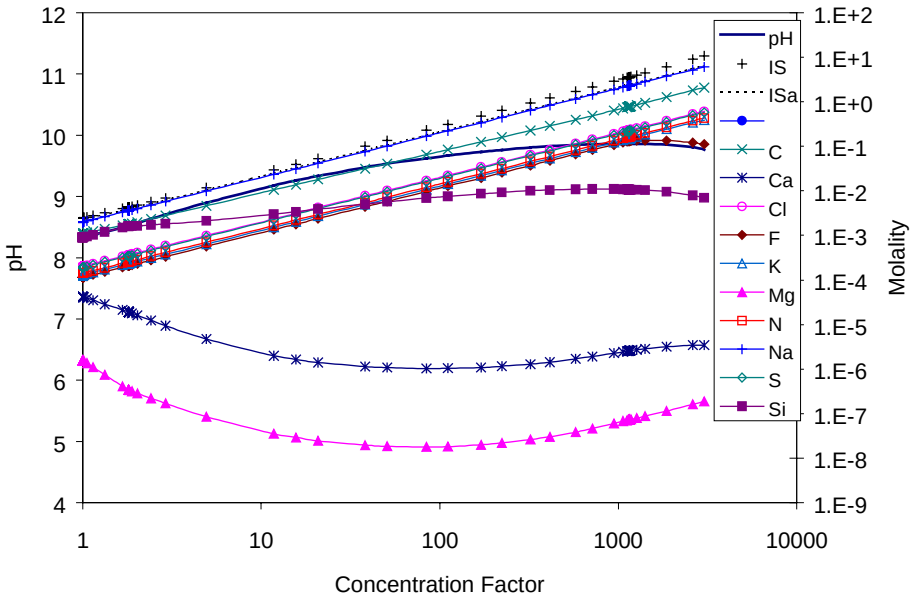

Figure 3. Aqueous Evaporative Evolution of In Situ J-13 Well Water at f_{CO2} of 10^{-3}

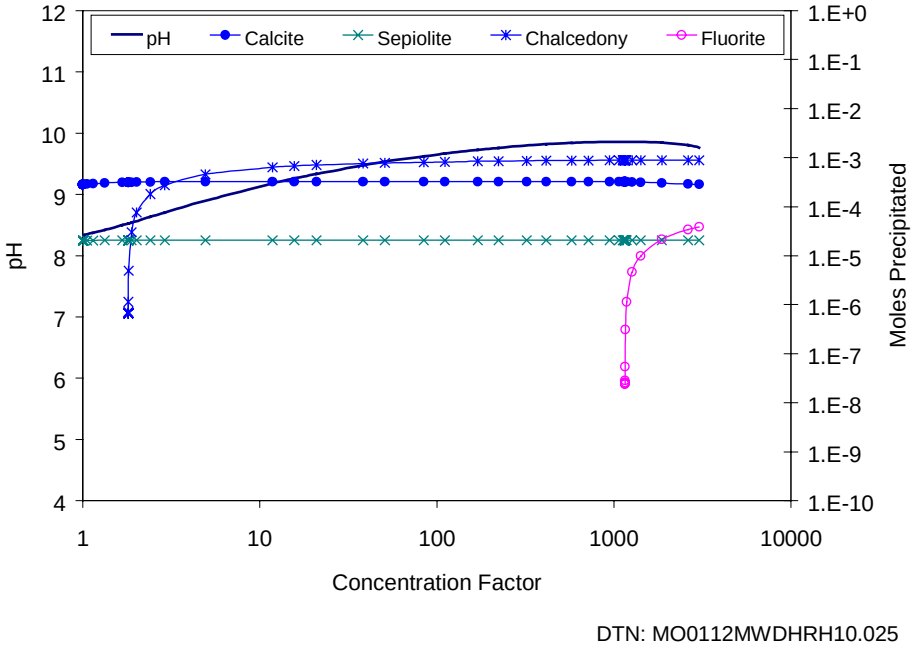

Figure 4. Mineral Evaporative Evolution of In Situ J-13 Well Water at f_{CO2} of 10^{-3}

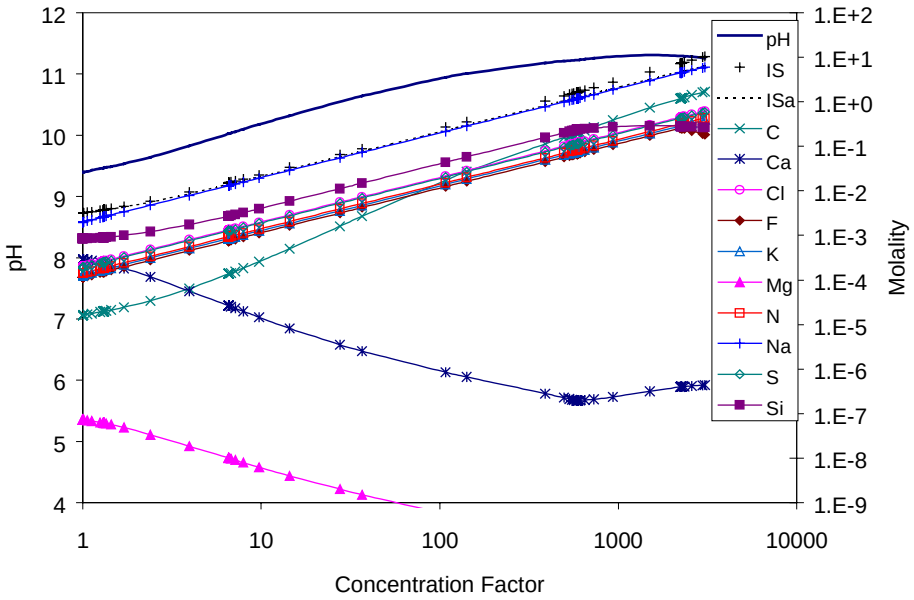

DTN: MO0112MWDHRH10.025

Figure 5. Aqueous Evaporative Evolution of In Situ J-13 Well Water at f_{CO2} of 10^{-6}

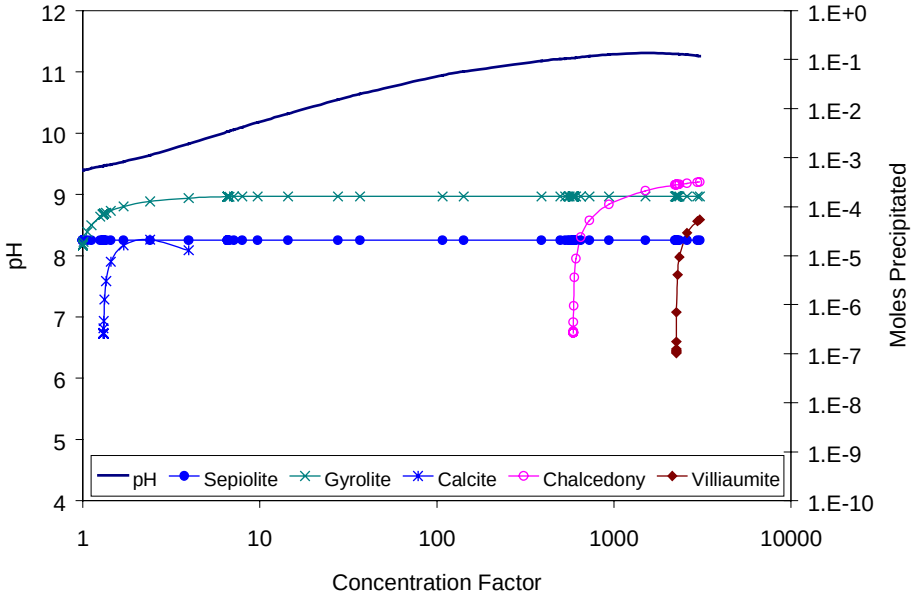

DTN: MO0112MWDHRH10.025

Figure 6. Mineral Evaporative Evolution of In Situ J-13 Well Water at f_{CO2} of 10^{-6}

6.1.2.2 Topopah Spring Tuff Pore Water (Water #2)

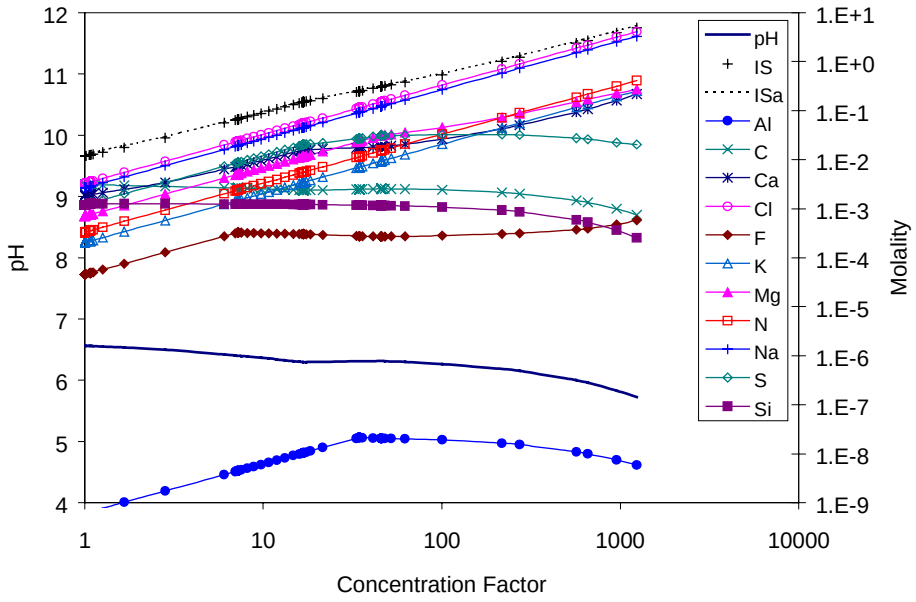

DTN: MO0112MWDHRH10.025

Figure 7. Aqueous Evaporative Evolution of Topopah Spring Tuff Pore Water at f_{CO2} of 10^{-1}

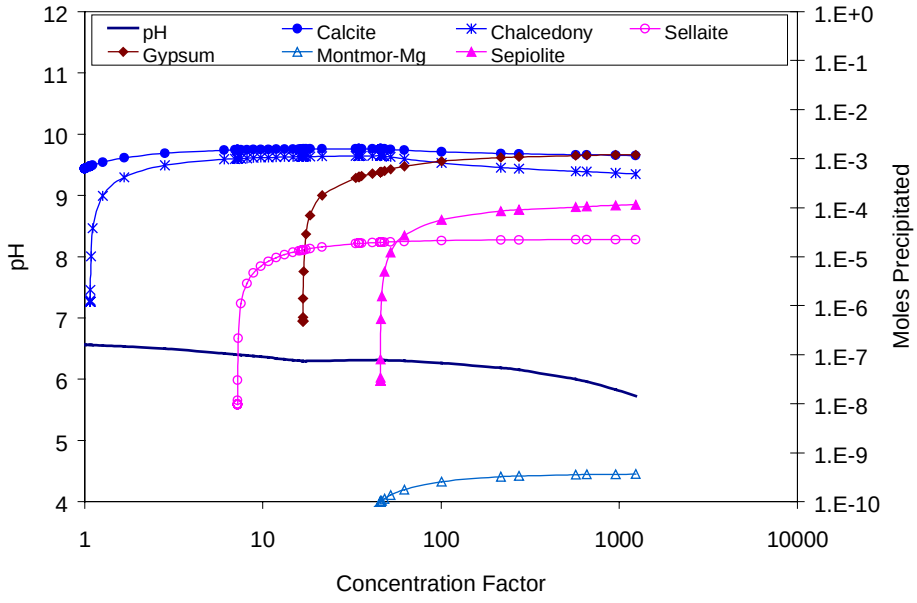

DTN: MO0112MWDHRH10.025

Figure 8. Mineral Evaporative Evolution of Topopah Spring Tuff Pore Water at f_{CO2} of 10^{-1}

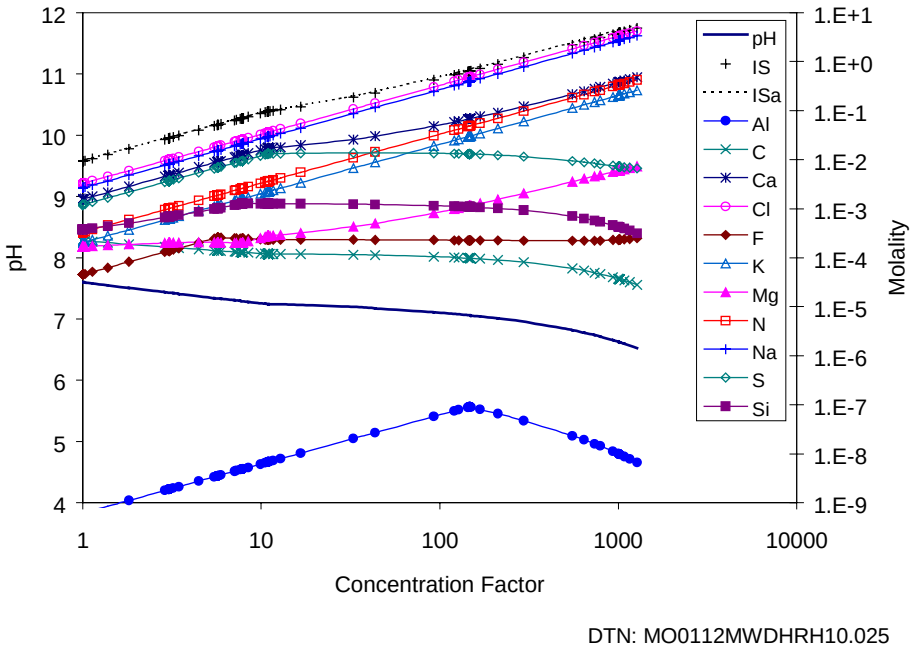

DTN: MO0112MWDHRH10.025

Figure 9. Aqueous Evaporative Evolution of Topopah Spring Tuff Pore Water at f_{CO2} of 10^{-3}

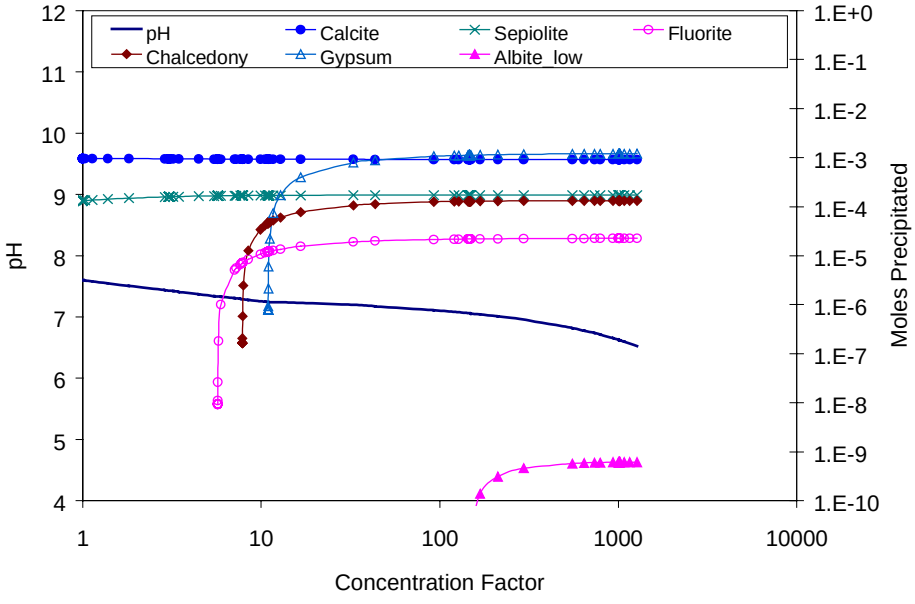

DTN: MO0112MWDHRH10.025

Figure 10. Mineral Evaporative Evolution of Topopah Spring Tuff Pore Water at f_{CO2} of 10^{-3}

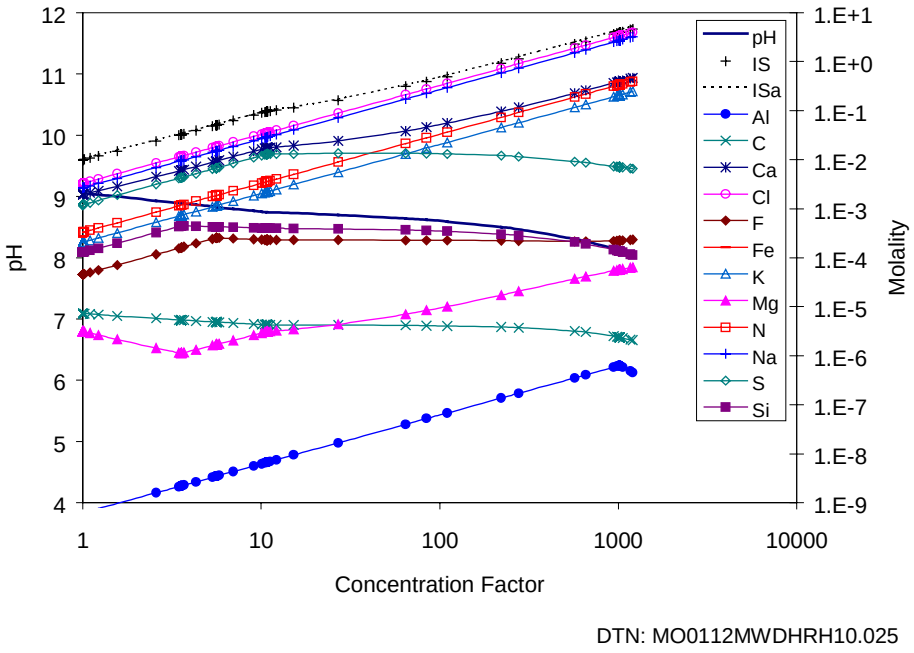

DTN: MO0112MWDHRH10.025

Figure 11. Aqueous Evaporative Evolution of Topopah Spring Tuff Pore Water at f_{CO2} of 10^{-6}

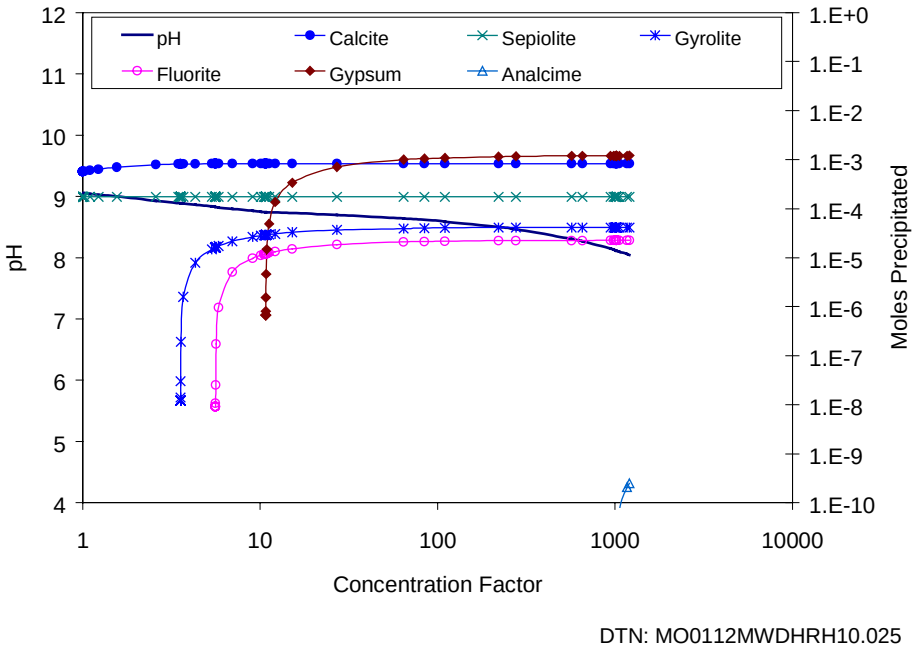

DTN: MO0112MWDHRH10.025

Figure 12. Mineral Evaporative Evolution of Topopah Spring Tuff Pore Water at f_{CO2} of 10^{-6}

6.1.2.3 UZ-14 Perched Water (Water #3)

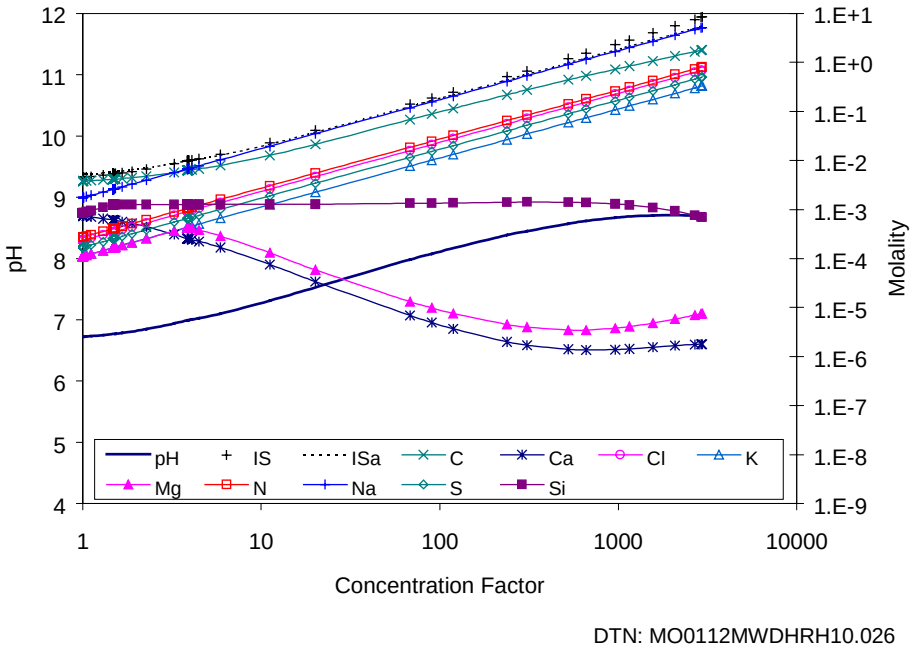

Figure 13. Aqueous Evaporative Evolution of Perched Water at f_{CO2} of 10^{-1}

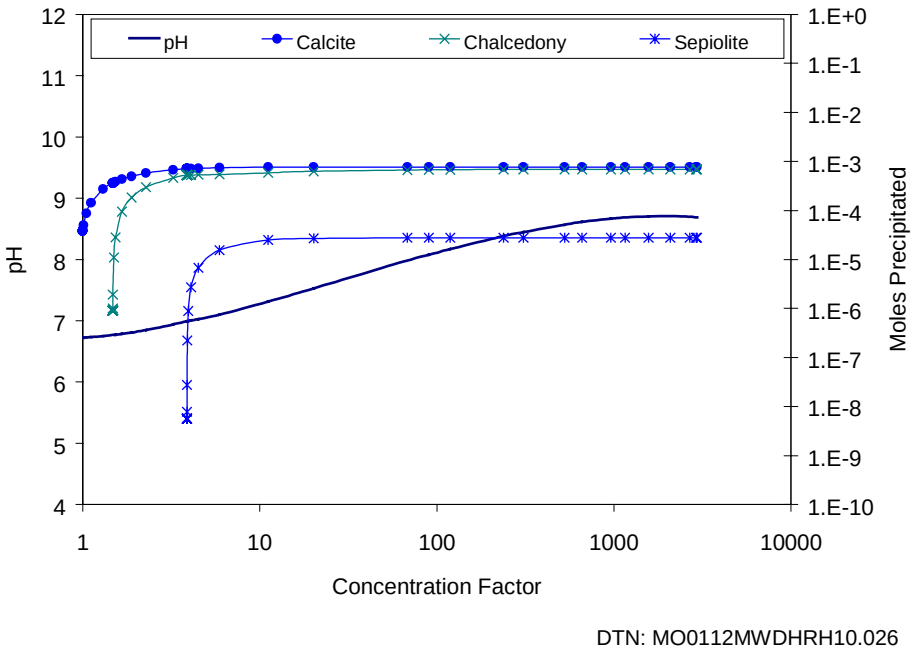

Figure 14. Mineral Evaporative Evolution of Perched Water at f_{CO2} of 10^{-1}

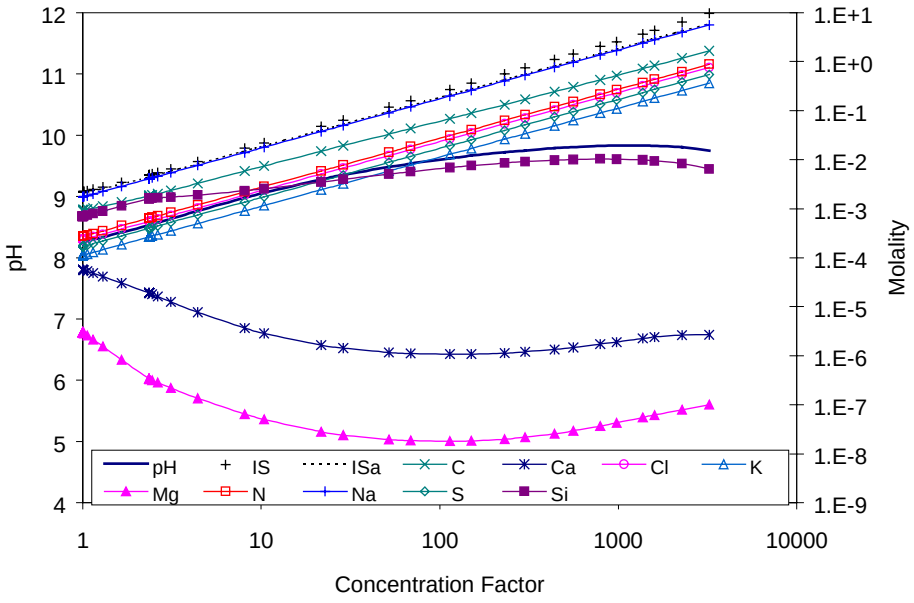

Figure 15. Aqueous Evaporative Evolution of Perched Water at f_{CO2} of 10^{-3}

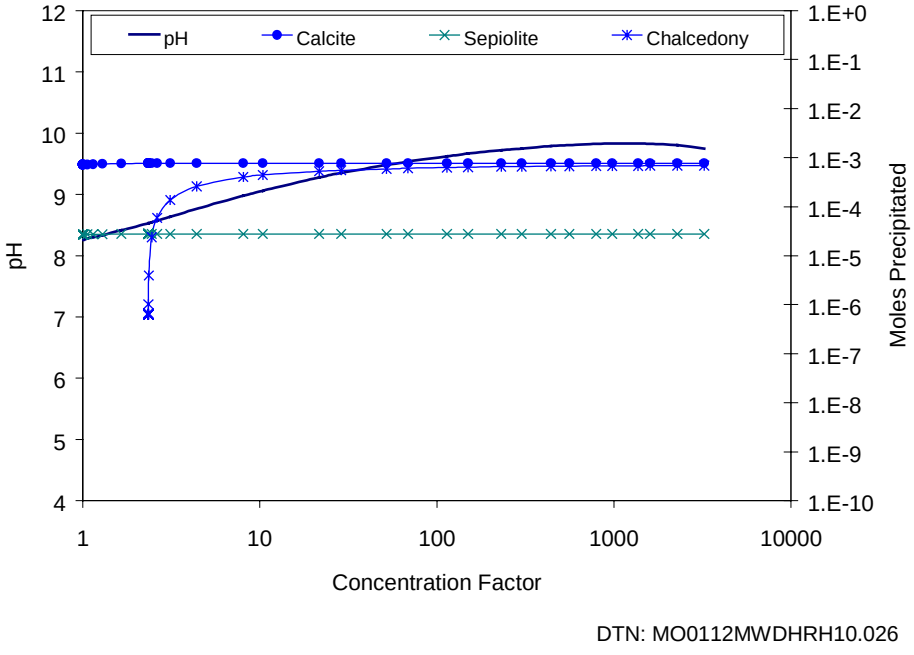

Figure 16. Mineral Evaporative Evolution of Perched Water at f_{CO2} of 10^{-3}

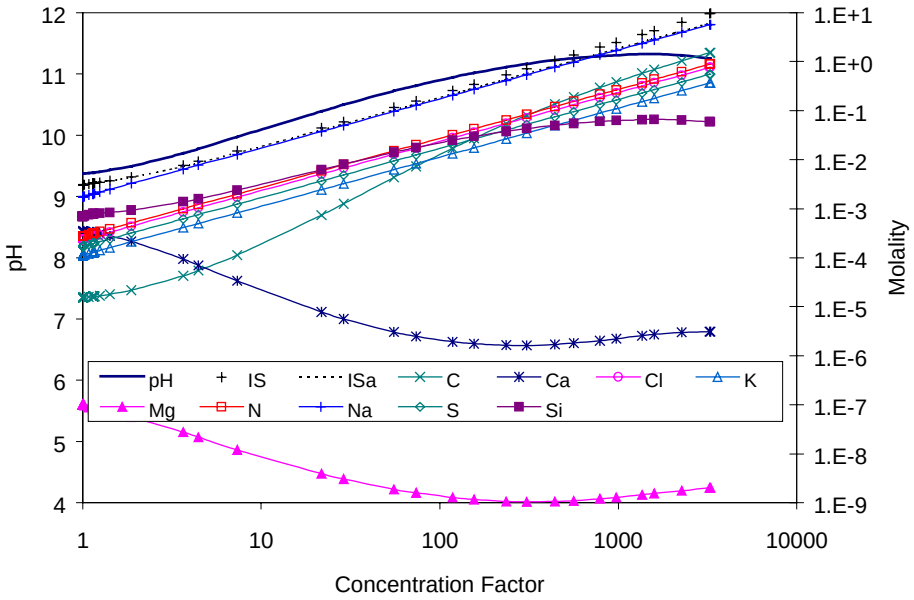

DTN: MO0112MWDHRH10.026

Figure 17. Aqueous Evaporative Evolution of Perched Water at f_{CO2} of 10^{-6}

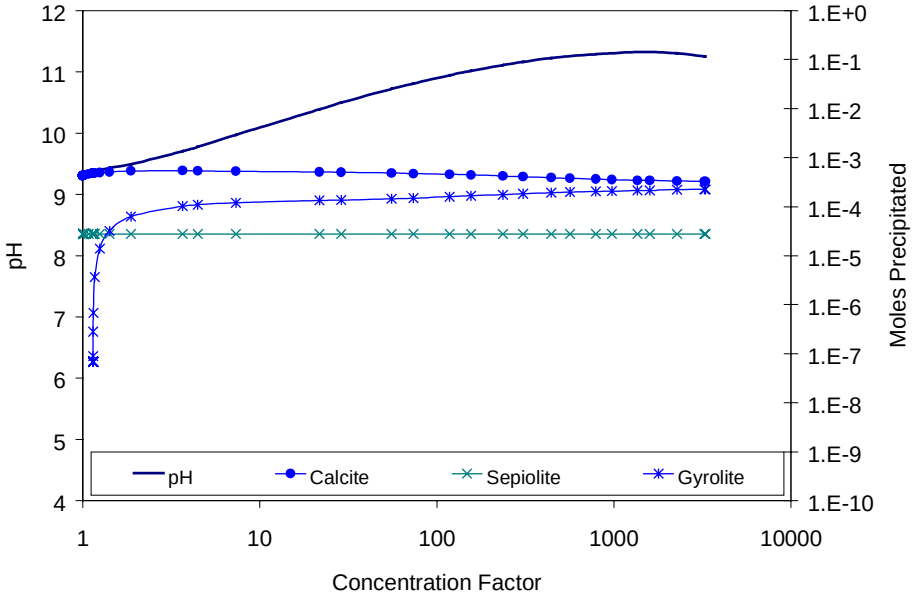

DTN: MO0112MWDHRH10.026

Figure 18. Mineral Evaporative Evolution of Perched Water at f_{CO2} of 10^{-6}

6.1.2.4 Single Heater Test Water (Water #4)

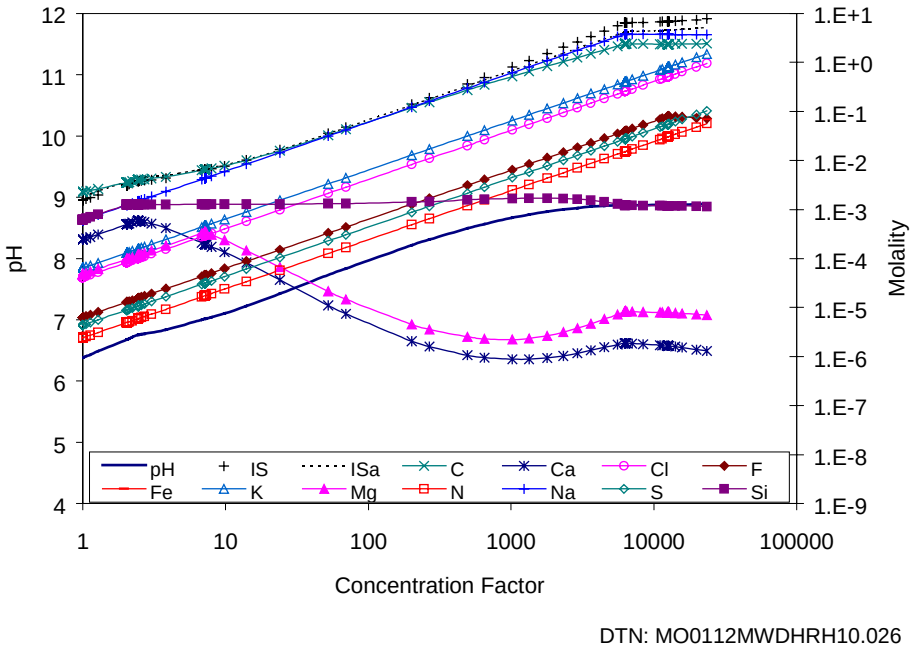

Figure 19. Aqueous Evaporative Evolution of Single Heater Test Water Sample at f_{CO2} of 10^{-1}

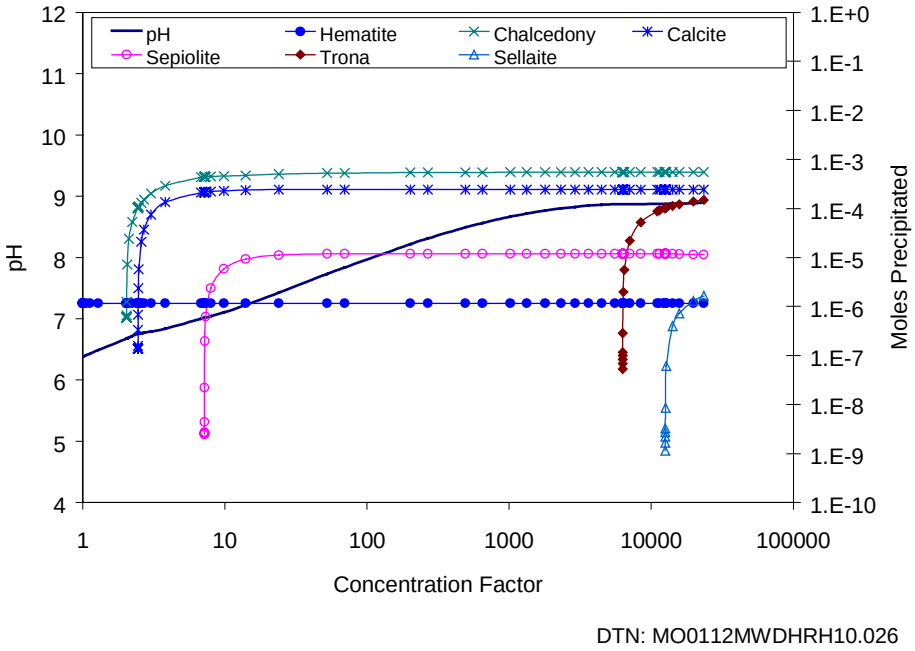

Figure 20. Mineral Evaporative Evolution of Single Heater Test Water Sample at f_{CO2} of 10^{-1}

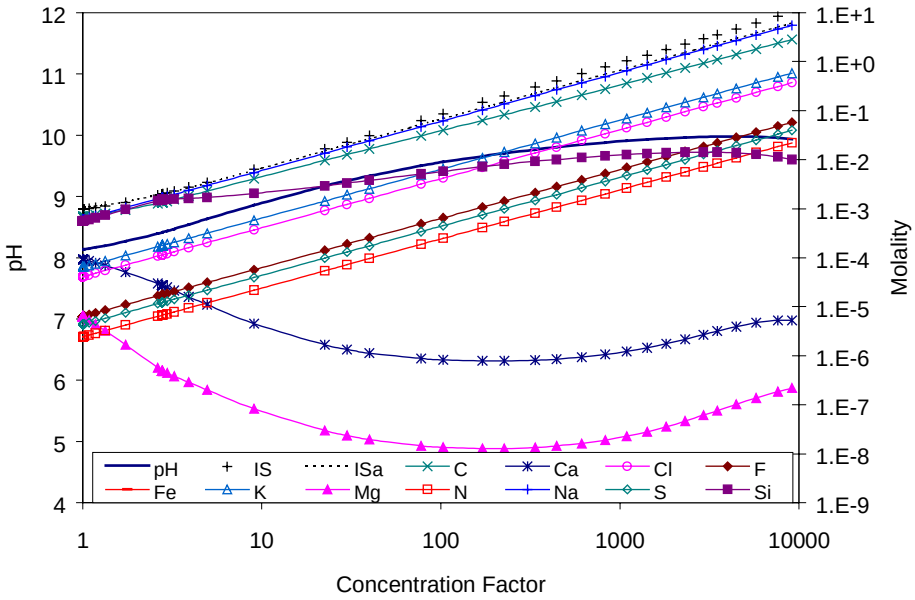

Figure 21. Aqueous Evaporative Evolution of Single Heater Test Water Sample at f_{CO2} of 10^{-3}

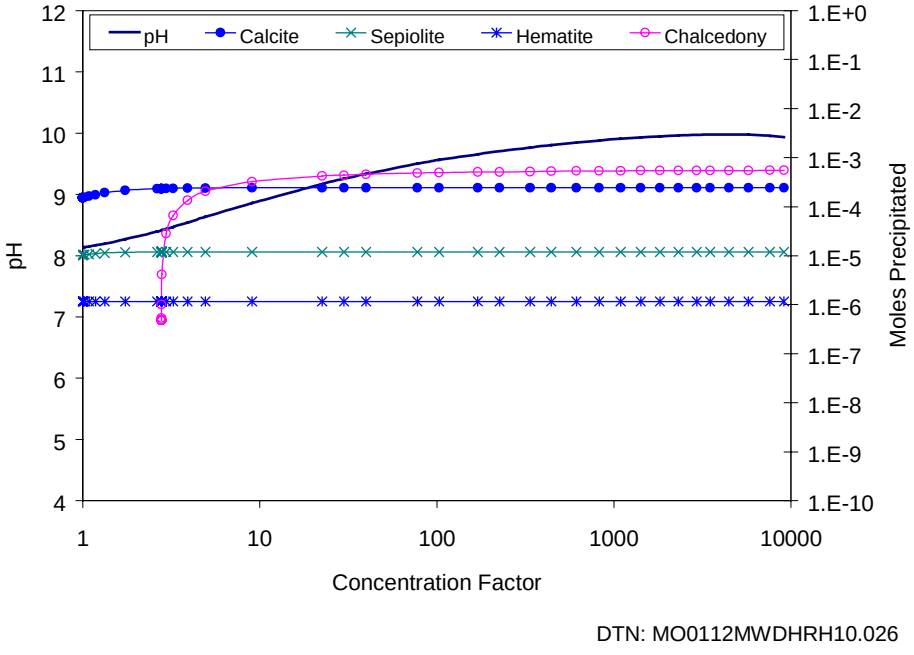

Figure 22. Mineral Evaporative Evolution of Single Heater Test Water Sample at f_{CO2} of 10^{-3}

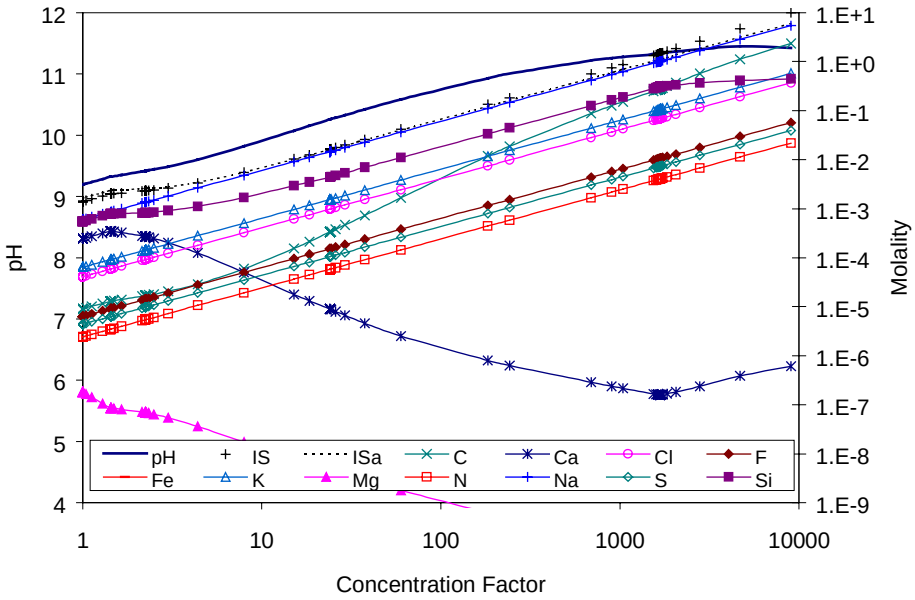

Figure 23. Aqueous Evaporative Evolution of Single Heater Test Water Sample at f_{CO2} of 10^{-6}

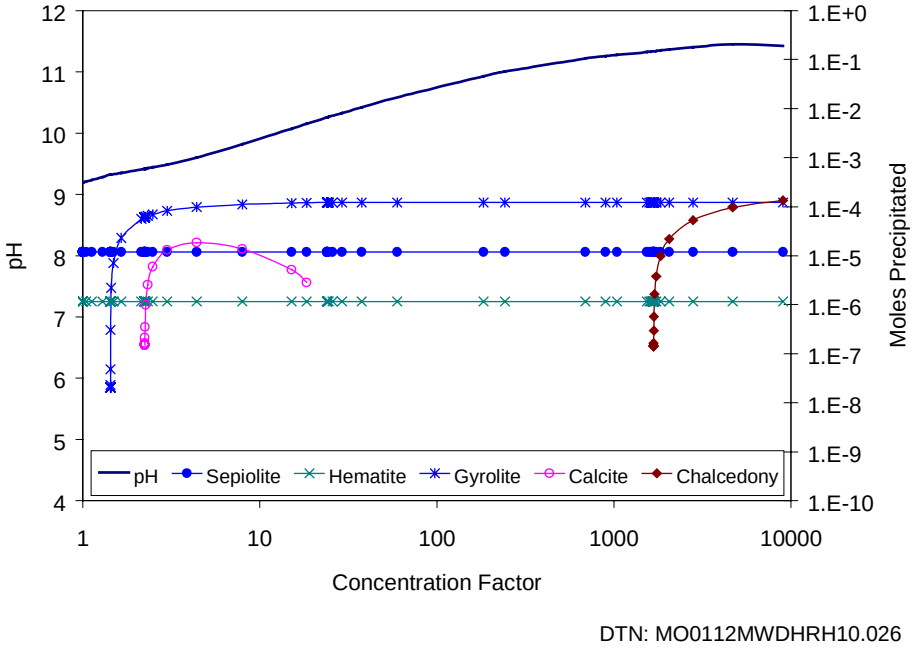

Figure 24. Mineral Evaporative Evolution of Single Heater Test Water Sample at f_{CO2} of 10^{-6}

6.1.2.5 Drift-Scale Heater Test Water (Water #5)

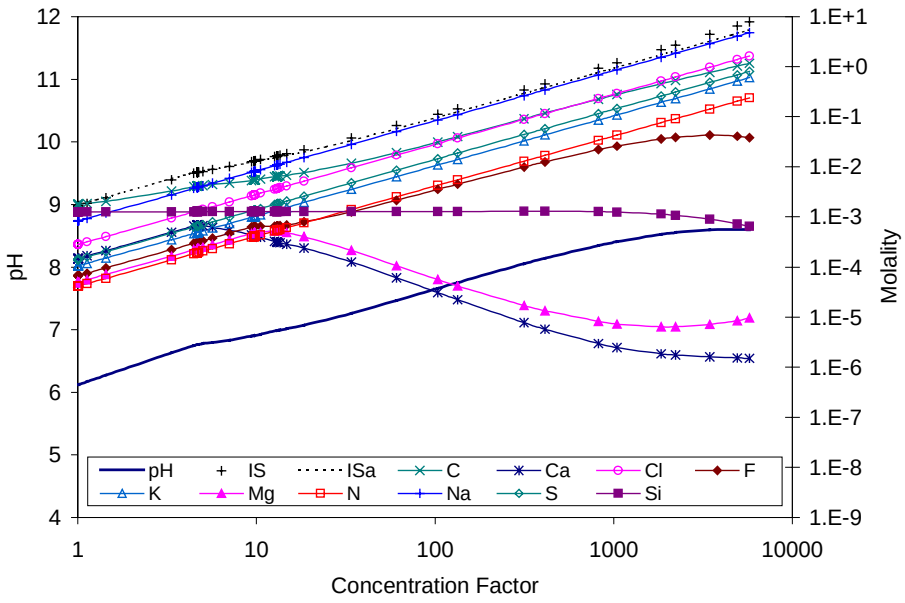

DTN: MO0112MWDHRH10.026

Figure 25. Aqueous Evaporative Evolution of Drift-Scale Heater Test Water Sample at f_{CO2} of 10^{-1}

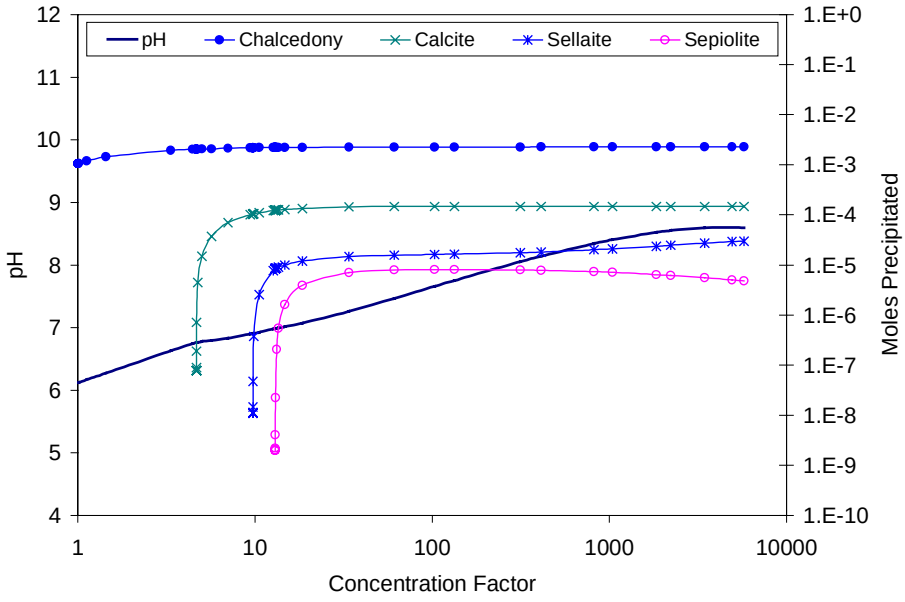

DTN: MO0112MWDHRH10.026

Figure 26. Mineral Evaporative Evolution of Drift-Scale Heater Test Water Sample at f_{CO2} of 10^{-1}

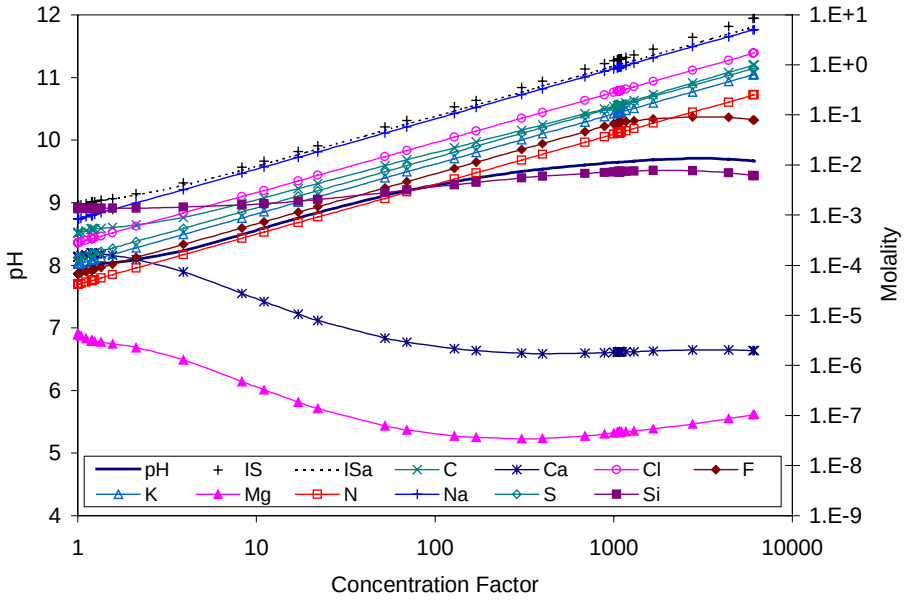

DTN: MO0112MWDHRH10.026

Figure 27. Aqueous Evaporative Evolution of Drift-Scale Heater Test Water Sample at f_{CO2} of 10^{-3}

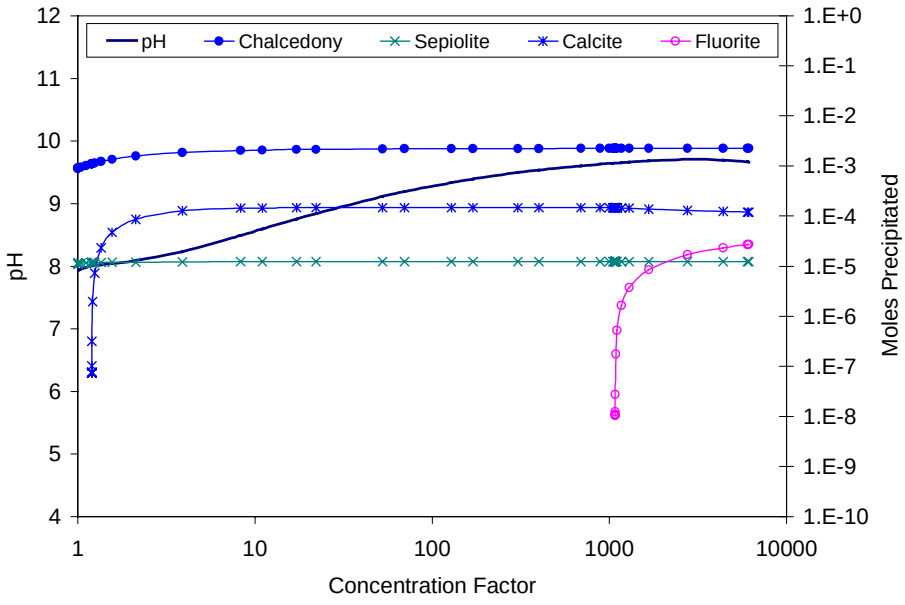

DTN: MO0112MWDHRH10.026

Figure 28. Mineral Evaporative Evolution of Drift-Scale Heater Test Water Sample at f_{CO2} of 10^{-3}

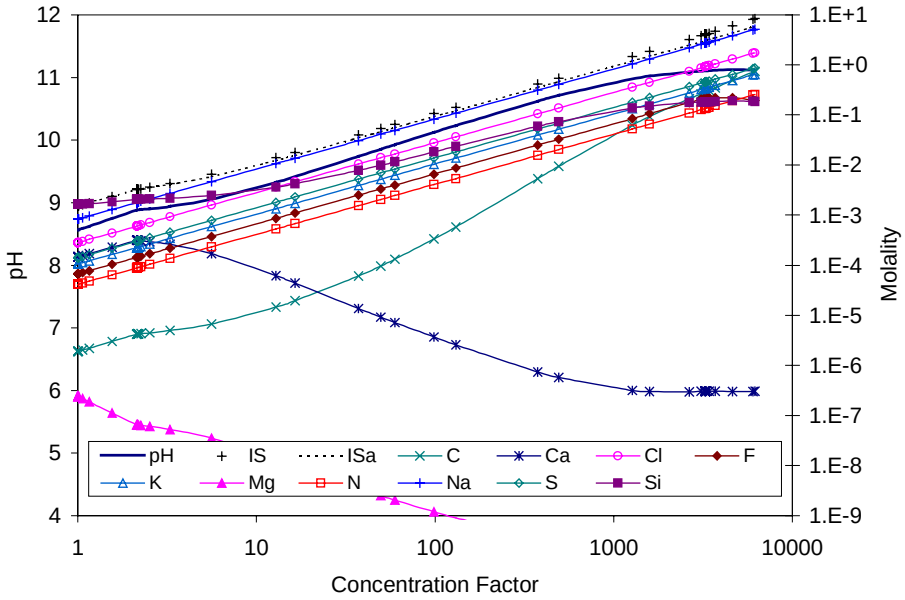

DTN: MO0112MWDHRH10.026

Figure 29. Aqueous Evaporative Evolution of Drift-Scale Heater Test Water Sample at f_{CO2} of 10^{-6}

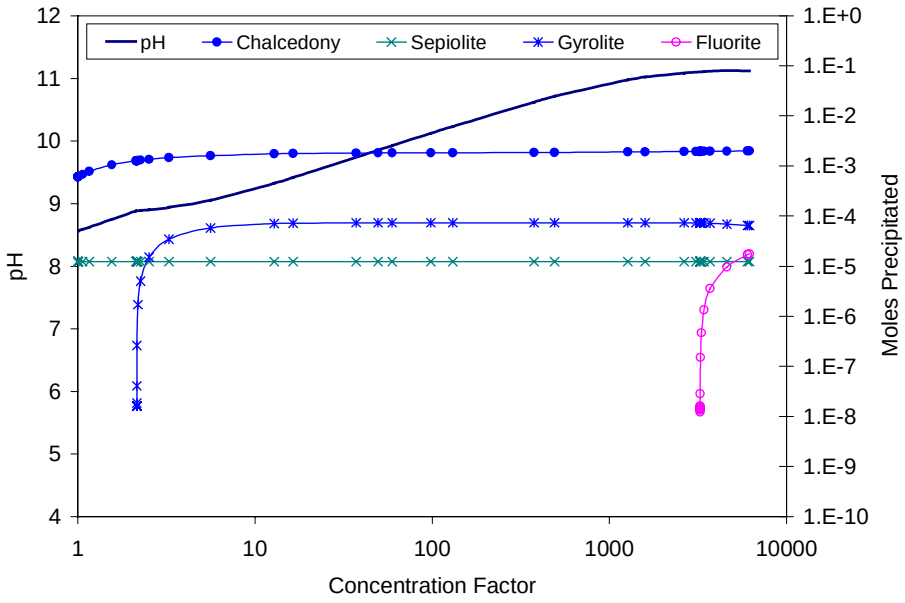

DTN: MO0112MWDHRH10.026

Figure 30. Mineral Evaporative Evolution of Drift-Scale Heater Test Water Sample at f_{CO2} of 10^{-6}

6.1.2.6 THC REV 00 Model Abstracted Seepage (Water #6)

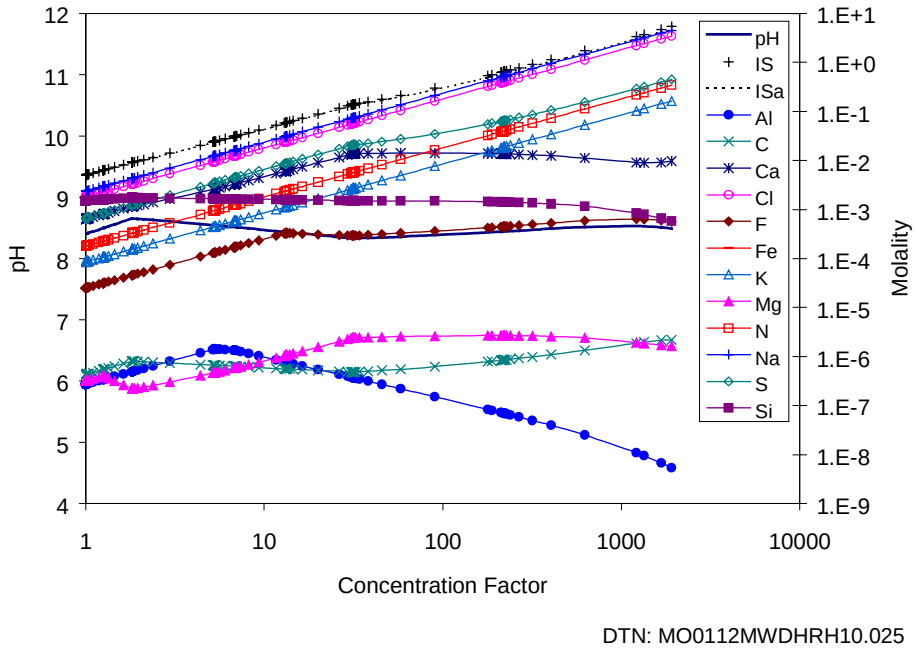

Figure 31. Aqueous Evaporative Evolution for THC Abstraction REV 00 Period 2

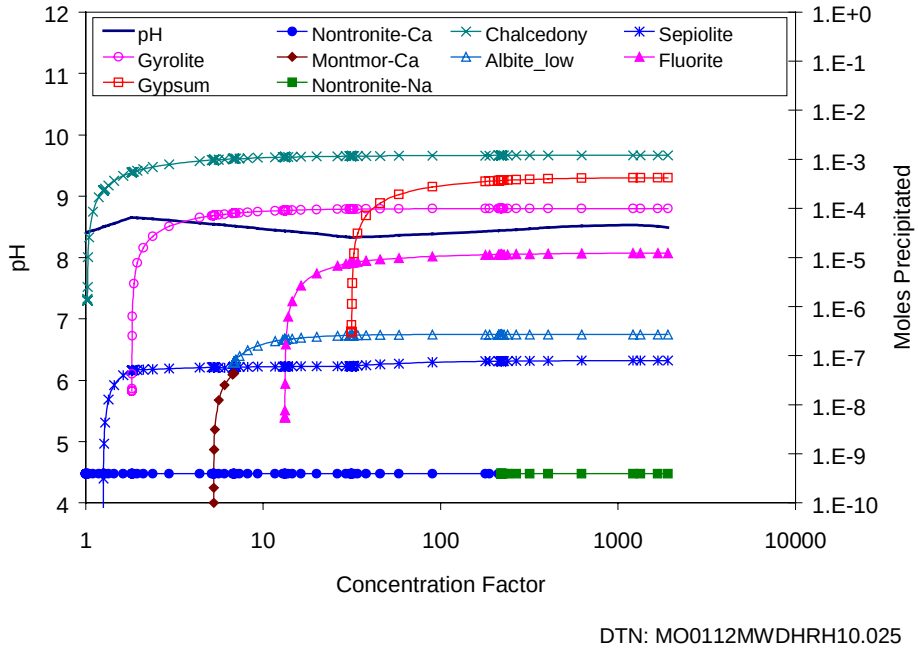

Figure 32. Mineral Evaporative Evolution for THC Abstraction REV 00 Period 2

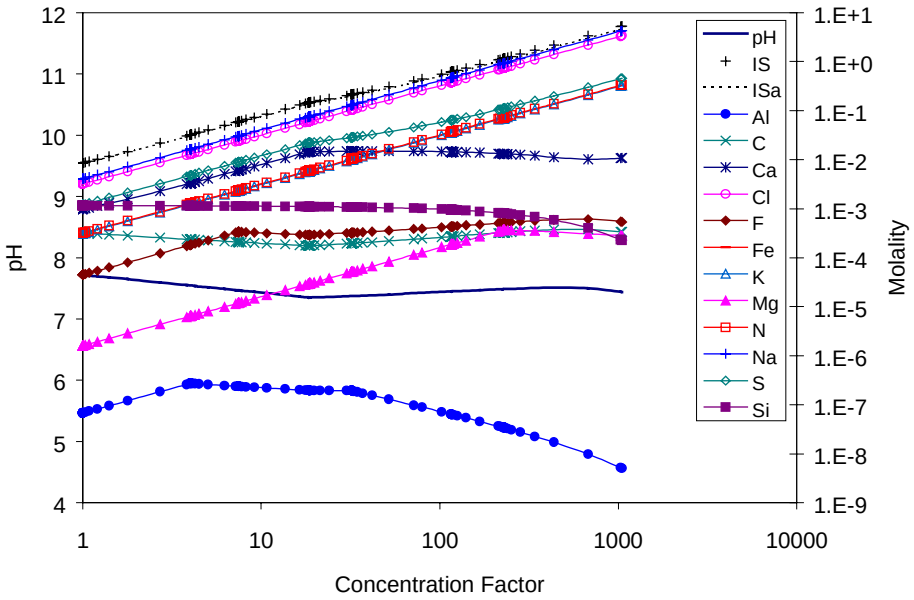

DTN: MO0112MWDHRH10.025

Figure 33. Aqueous Evaporative Evolution for THC Abstraction REV 00 Period 3

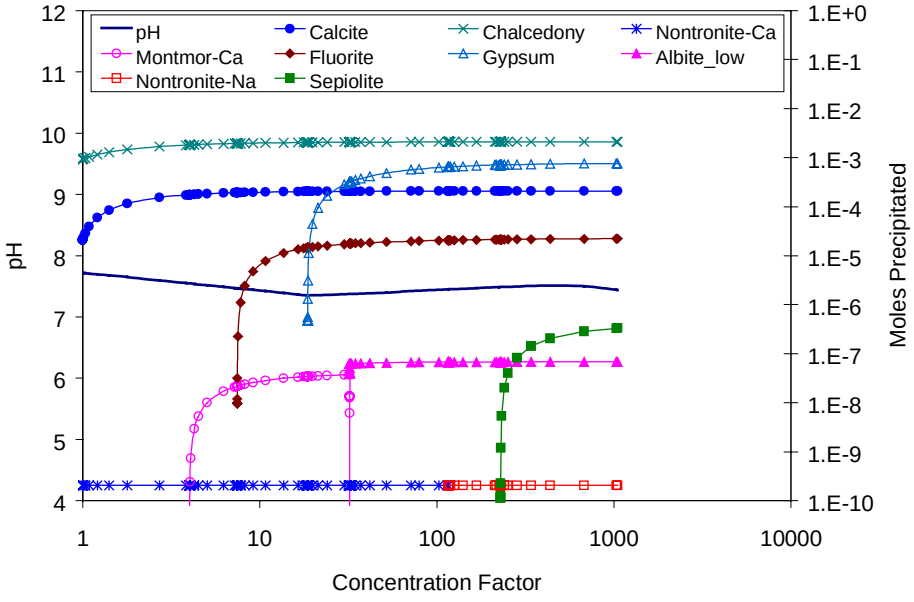

DTN: MO0112MWDHRH10.025

Figure 34. Mineral Evaporative Evolution for THC Abstraction REV 00 Period 3

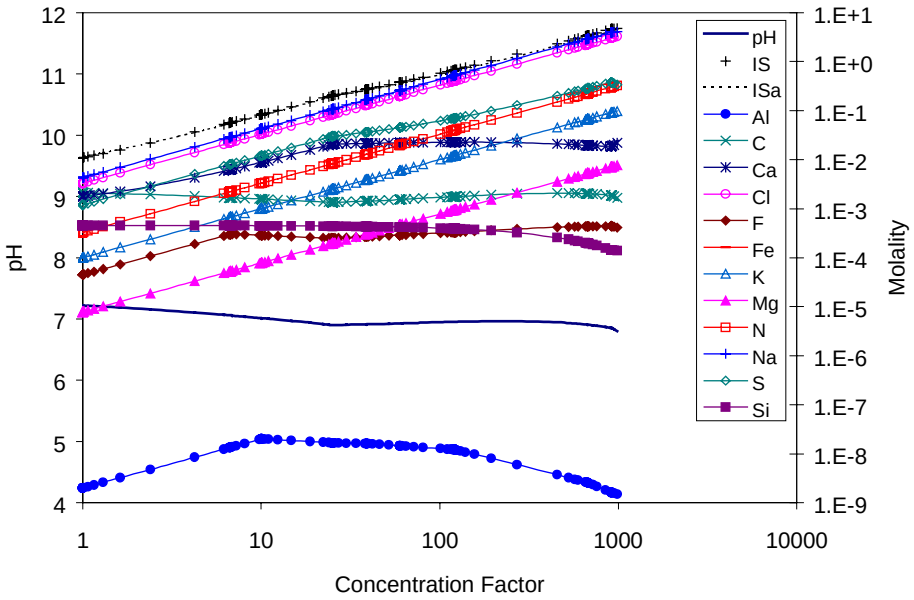

Figure 35. Aqueous Evaporative Evolution for THC Abstraction REV 00 Period 4

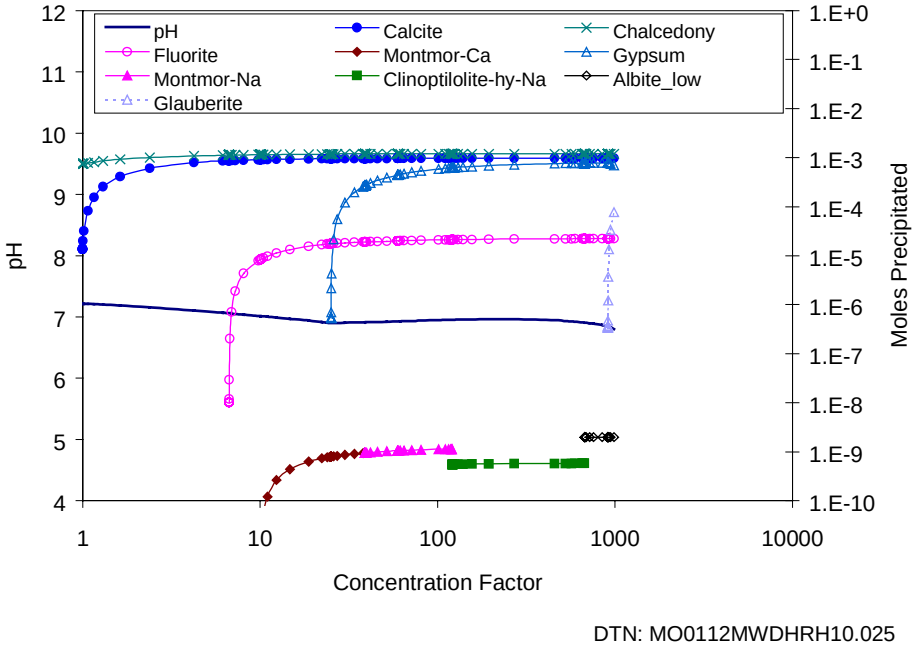

Figure 36. Mineral Evaporative Evolution for THC Abstraction REV 00 Period 4

6.1.2.7 THC REV 01 Model Abstracted Seepage (Water #7)

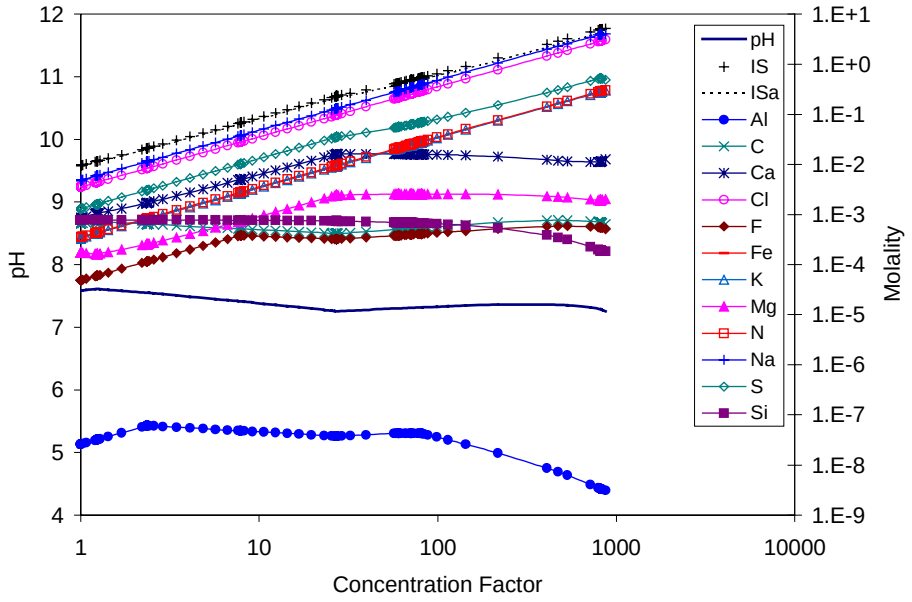

DTN: MO0112MWDTHC12.024

Figure 37. Aqueous Evaporative Evolution for the REV 01 THC Model Abstraction for Seepage at the Crown of the Drift in the Tptpmn Lithology, Period 1

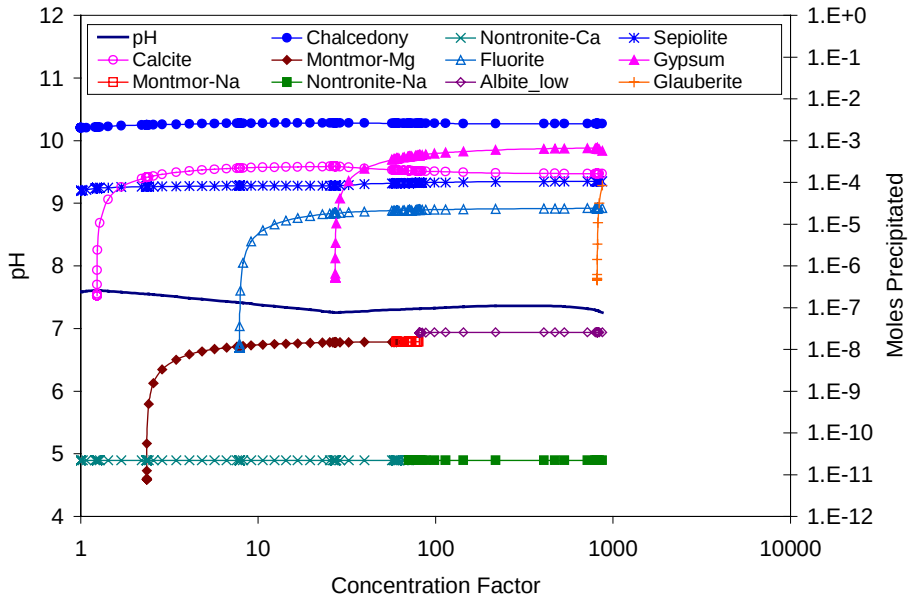

DTN: MO0112MWDTHC12.024

Figure 38. Mineral Evaporative Evolution for the REV 01 THC Model Abstraction for Seepage at the Crown of the Drift in the Tptpmn Lithology, Period 1

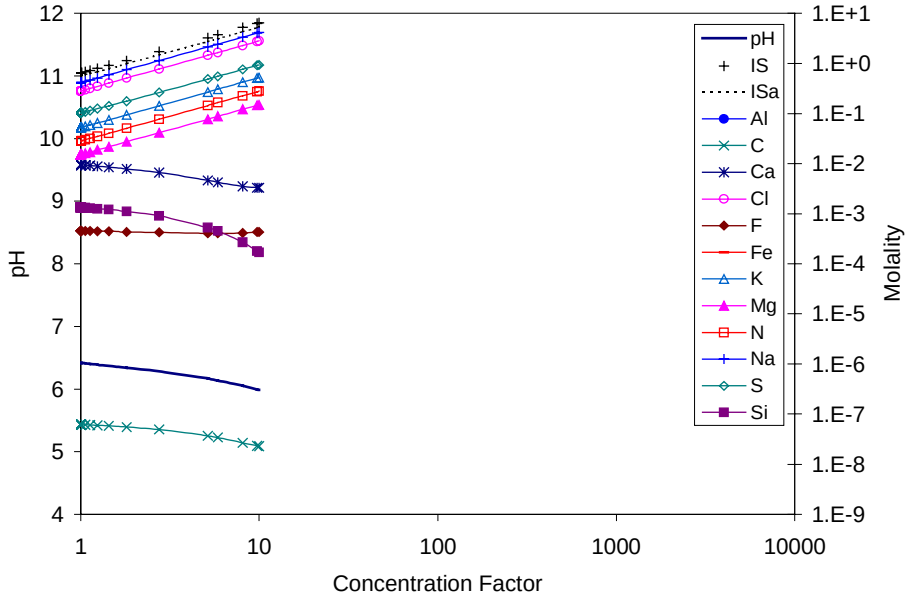

DTN: MO0112MWDTHC12.024

Figure 39. Aqueous Evaporative Evolution for the REV 01 THC Model Abstraction for Seepage at the Crown of the Drift in the Tptpmn Lithology, Period 2

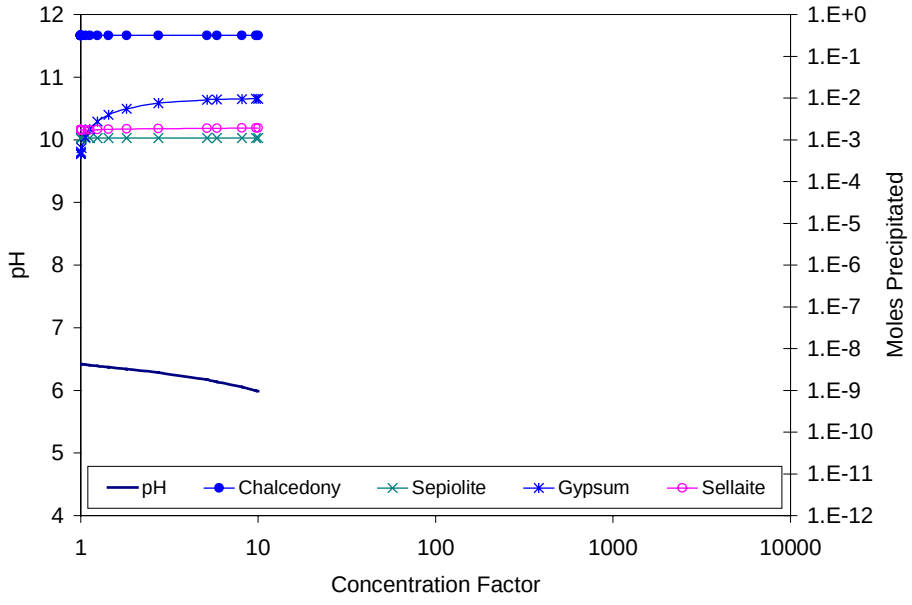

DTN: MO0112MWDTHC12.024

Figure 40. Mineral Evaporative Evolution for the REV 01 THC Model Abstraction for Seepage at the Crown of the Drift in the Tptpmn Lithology, Period 2

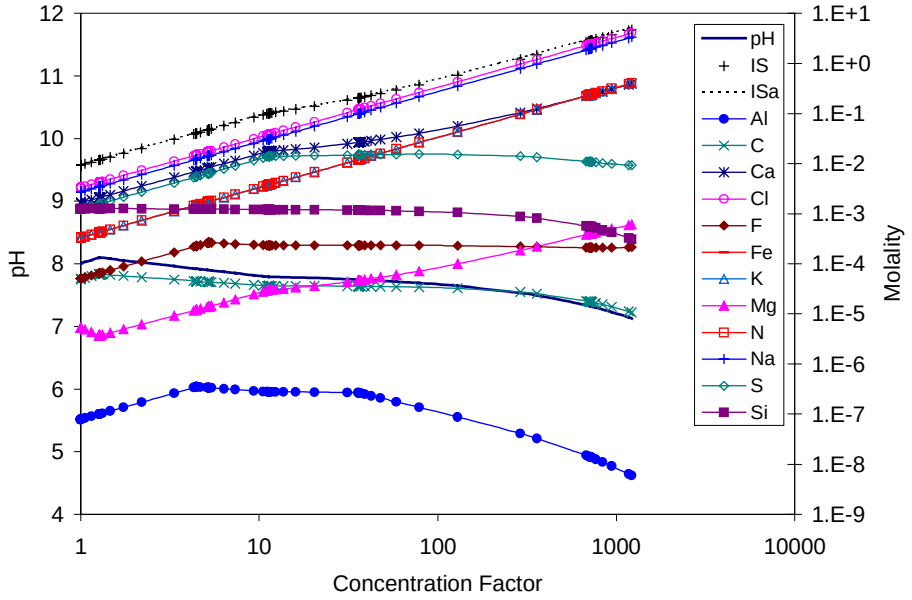

DTN: MO0112MWDTHC12.024

Figure 41. Aqueous Evaporative Evolution for the REV 01 THC Model Abstraction for Seepage at the Crown of the Drift in the Tptpmn Lithology, Period 3

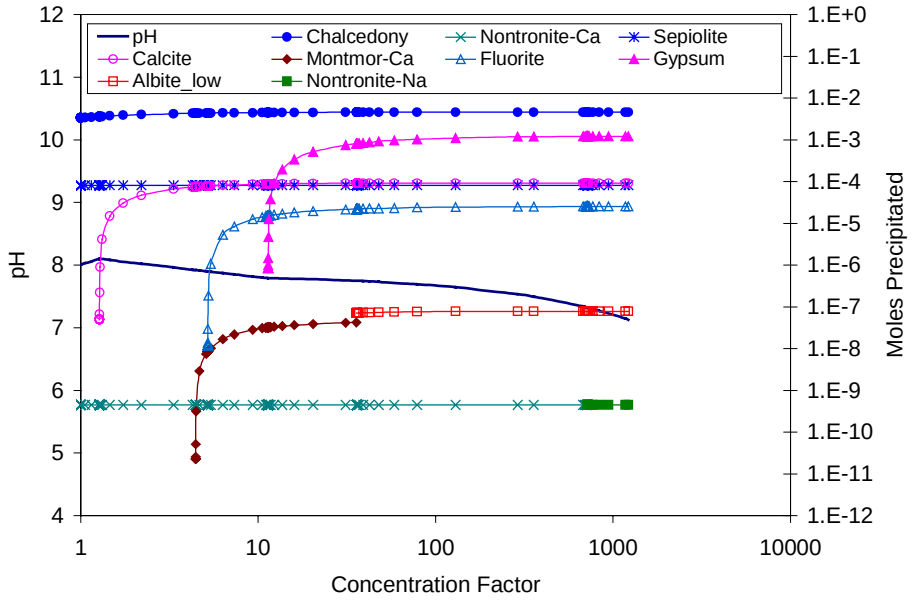

DTN: MO0112MWDTHC12.024

Figure 42. Mineral Evaporative Evolution for the REV 01 THC Model Abstraction for Seepage at the Crown of the Drift in the Tptpmn Lithology, Period 3

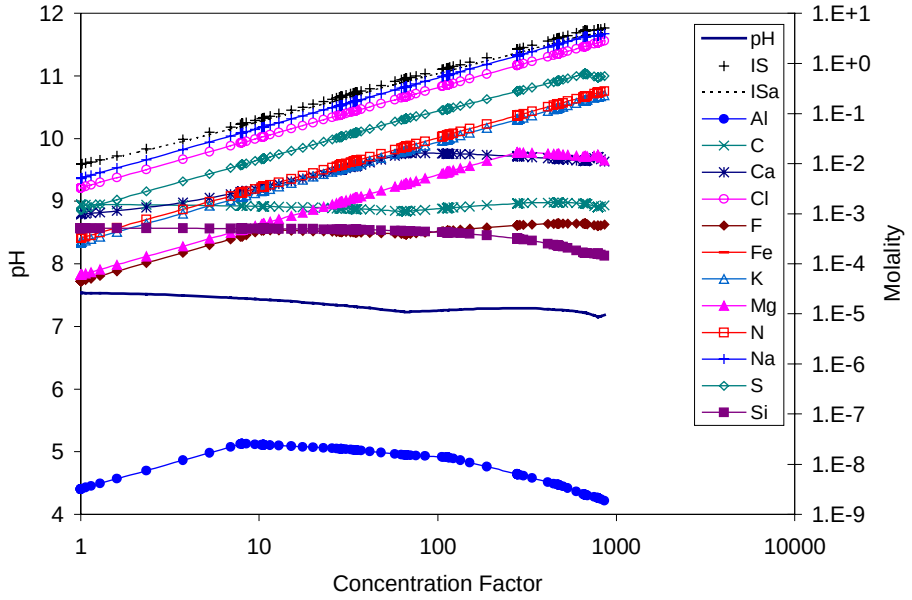

DTN: MO0112MWDTHC12.024

Figure 43. Aqueous Evaporative Evolution for the REV 01 THC Model Abstraction for Seepage at the Crown of the Drift in the Tptpmn Lithology, Period 4

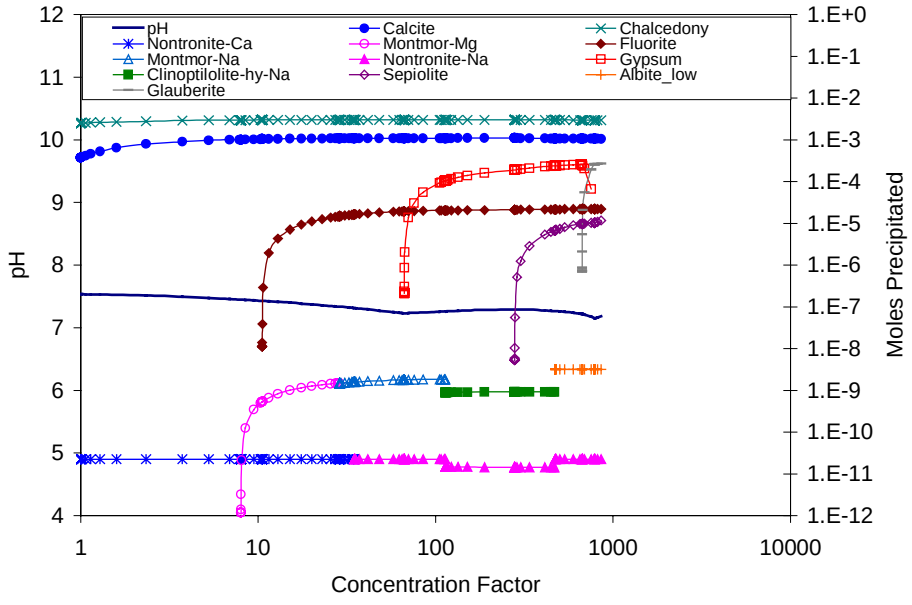

DTN: MO0112MWDTHC12.024

Figure 44. Mineral Evaporative Evolution for the REV 01 THC Model Abstraction for Seepage at the Crown of the Drift in the Tptpmn Lithology, Period 4

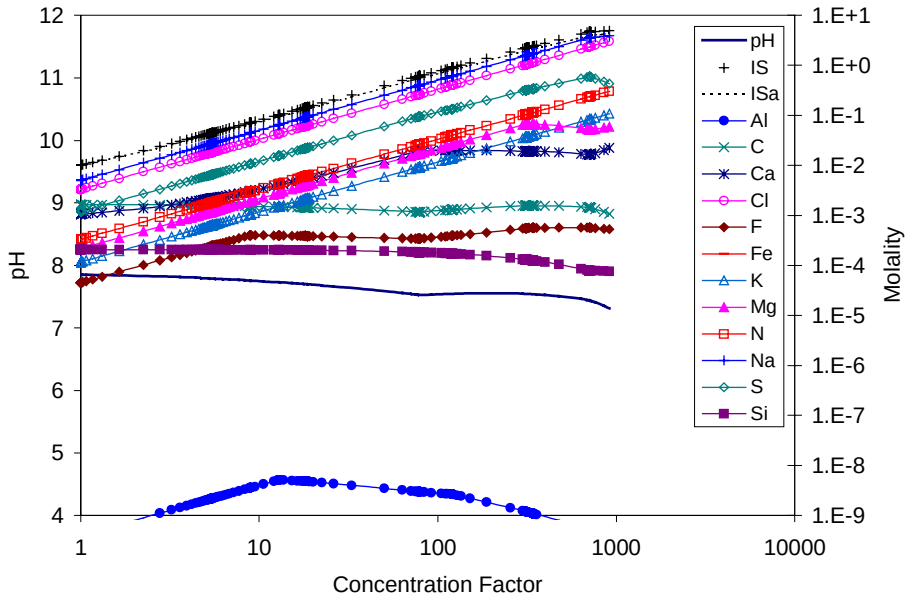

DTN: MO0112MWDTHC12.024

Figure 45. Aqueous Evaporative Evolution for the REV 01 THC Model Abstraction for Seepage at the Crown of the Drift in the Tptpmn Lithology, Period 5

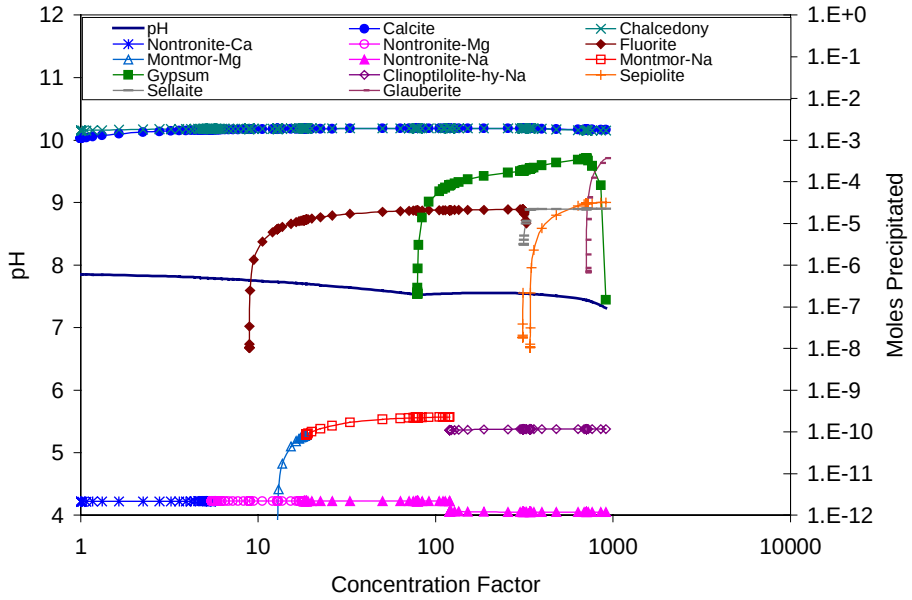

DTN: MO0112MWDTHC12.024

Figure 46. Mineral Evaporative Evolution for the REV 01 THC Model Abstraction for Seepage at the Crown of the Drift in the Tptpmn Lithology, Period 5

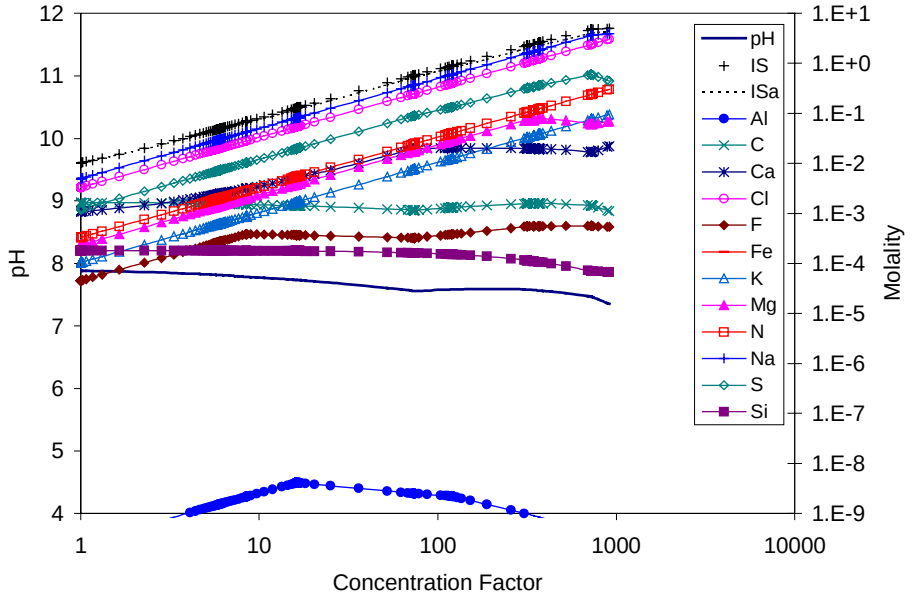

DTN: MO0112MWDTHC12.024

Figure 47. Aqueous Evaporative Evolution for the REV 01 THC Model Abstraction for Matrix Imbibition into the Invert in the Tptpmn Lithology, Period 6

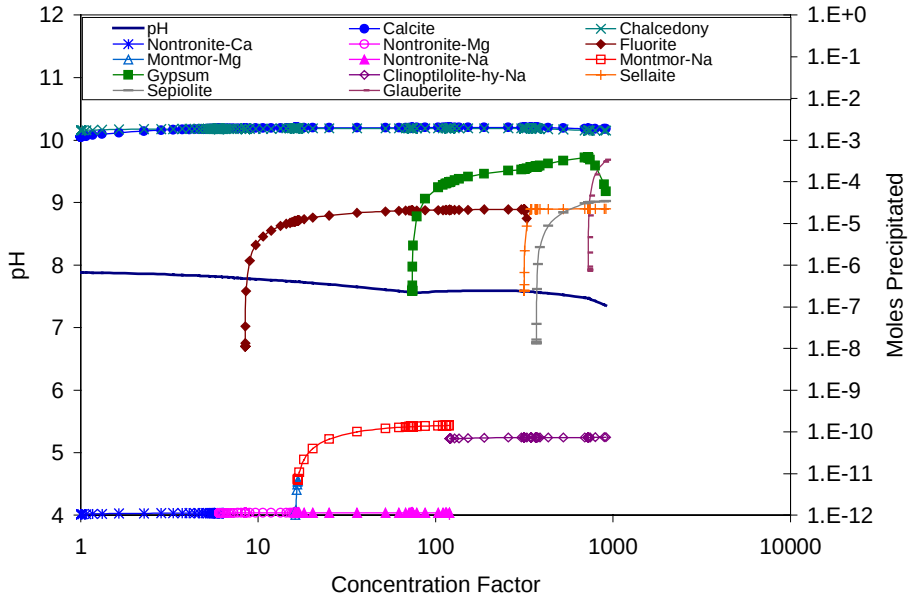

DTN: MO0112MWDTHC12.024

Figure 48. Mineral Evaporative Evolution for the REV 01 THC Model Abstraction for Matrix Imbibition into the Invert in the Tptpmn Lithology, Period 6

6.1.2.8 Cement Grout Leachate (Water #8)

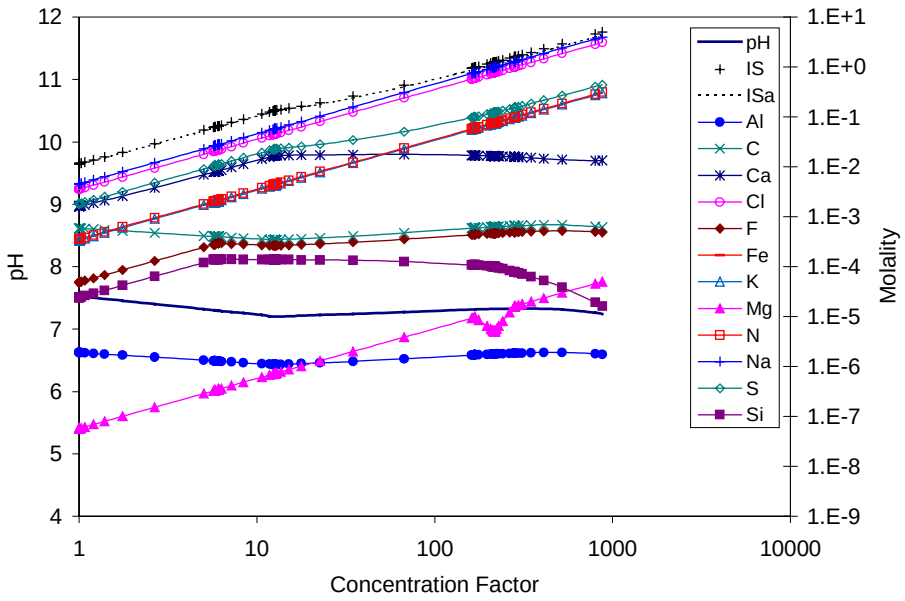

DTN: MO0112MWDHRH10.025

Figure 49. Aqueous Evaporative Evolution of Cement Leachate for the REV 01 THC Model Abstraction at the Crown of the Drift in the Tptpmn Lithology, Period 1

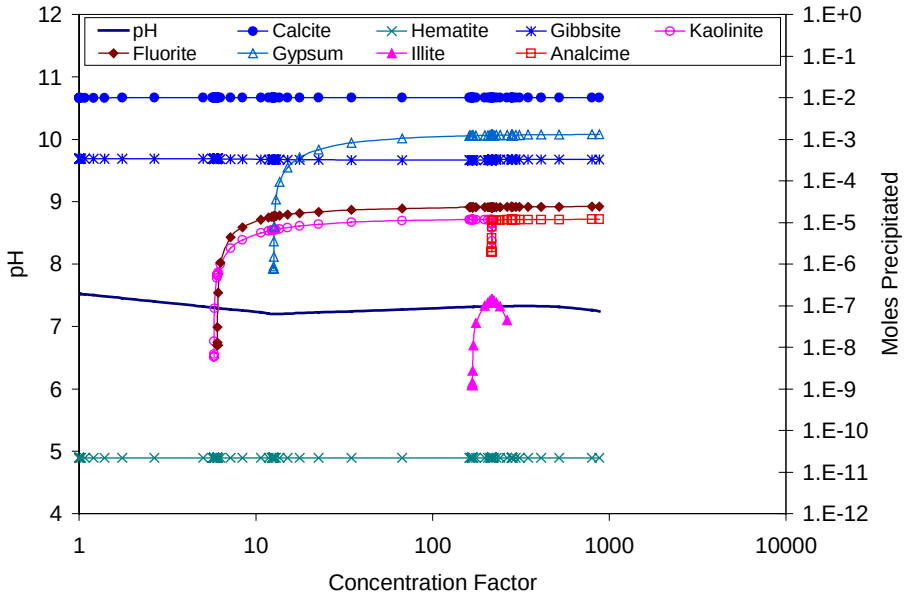

DTN: MO0112MWDHRH10.025

Figure 50. Mineral Evaporative Evolution of Cement Leachate for the REV 01 THC Model Abstraction at the Crown of the Drift in the Tptpmn Lithology, Period 1

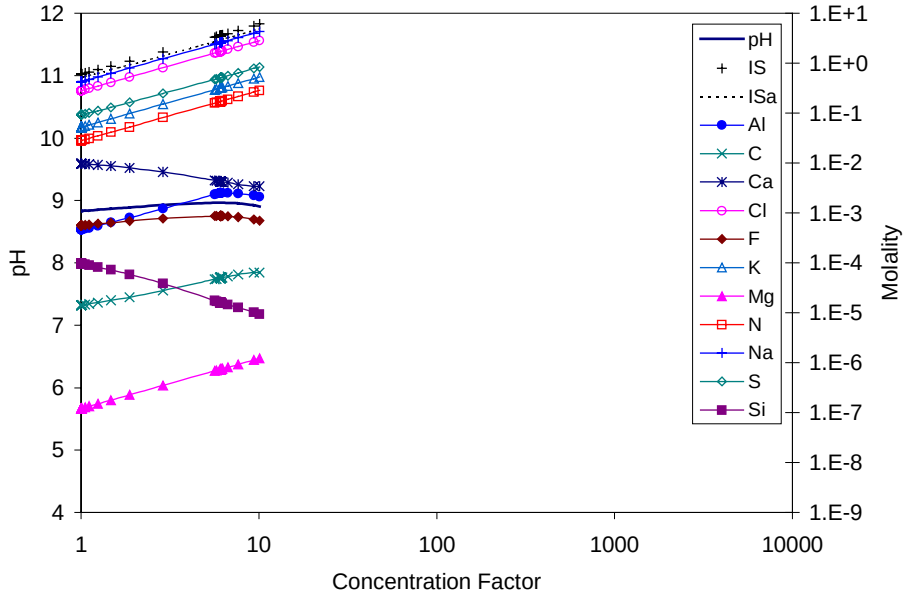

DTN: MO0112MWDHRH10.025

Figure 51. Aqueous Evaporative Evolution of Cement Leachate for the REV 01 THC Model Abstraction at the Crown of the Drift in the Tptpmn Lithology, Period 2

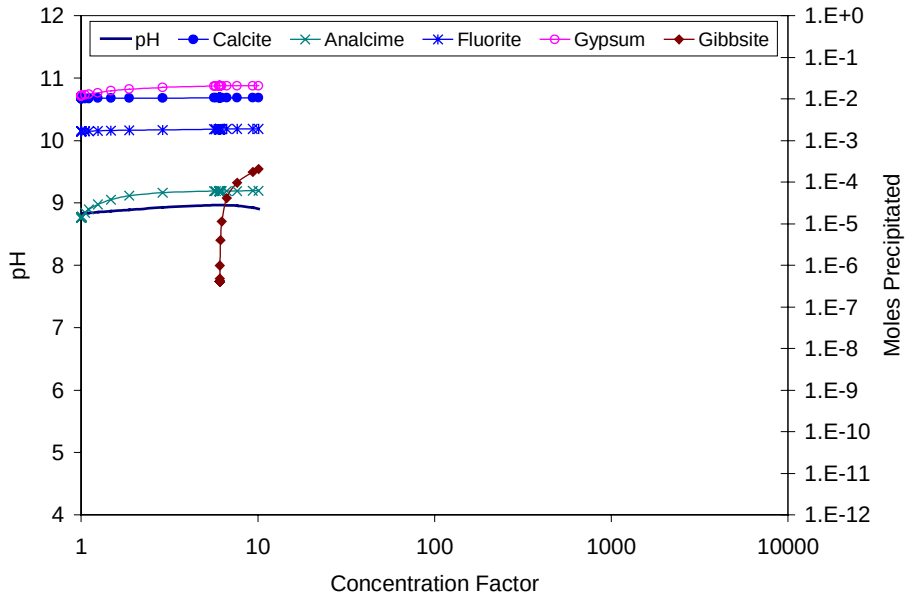

DTN: MO0112MWDHRH10.025

Figure 52. Mineral Evaporative Evolution of Cement Leachate for the REV 01 THC Model Abstraction at the Crown of the Drift in the Tptpmn Lithology, Period 2

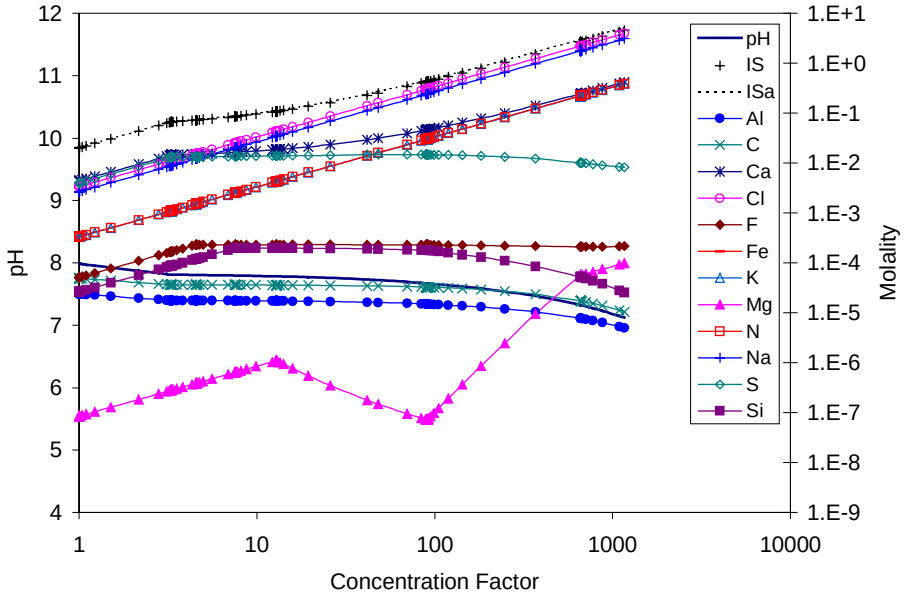

DTN: MO0112MWDHRH10.025

Figure 53. Aqueous Evaporative Evolution of Cement Leachate for the REV 01 THC Model Abstraction at the Crown of the Drift in the Tptpmn Lithology, Period 3

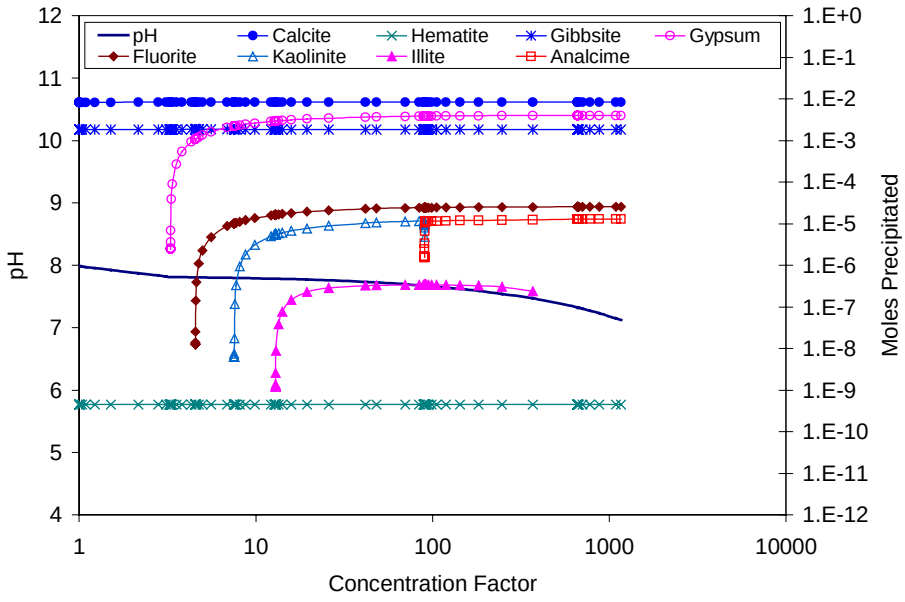

DTN: MO0112MWDHRH10.025

Figure 54. Mineral Evaporative Evolution of Cement Leachate for the REV 01 THC Model Abstraction at the Crown of the Drift in the Tptpmn Lithology, Period 3

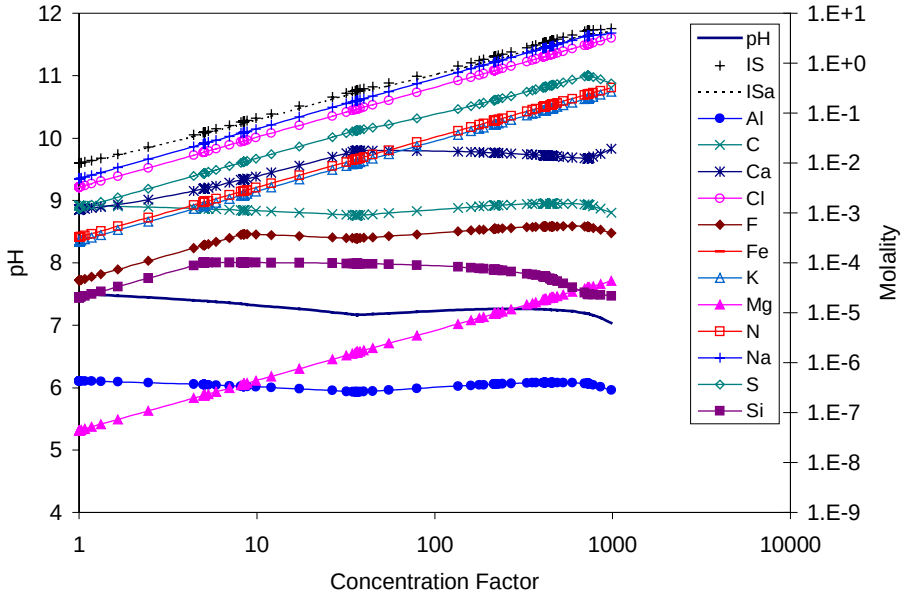

DTN: MO0112MWDHRH10.025

Figure 55. Aqueous Evaporative Evolution of Cement Leachate for the REV 01 THC Model Abstraction at the Crown of the Drift in the Tptpmn Lithology, Period 4

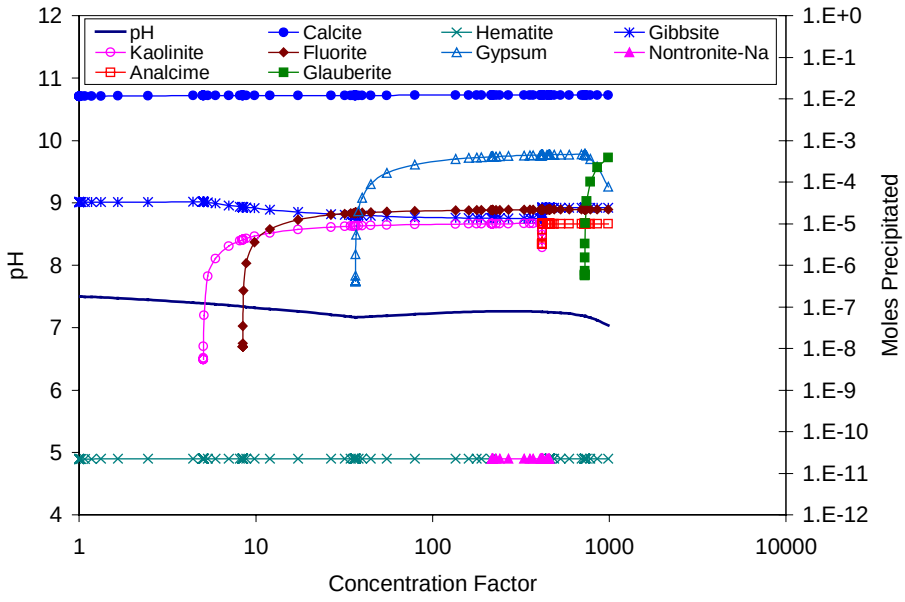

DTN: MO0112MWDHRH10.025

Figure 56. Mineral Evaporative Evolution of Cement Leachate for the REV 01 THC Model Abstraction at the Crown of the Drift in the Tptpmn Lithology, Period 4

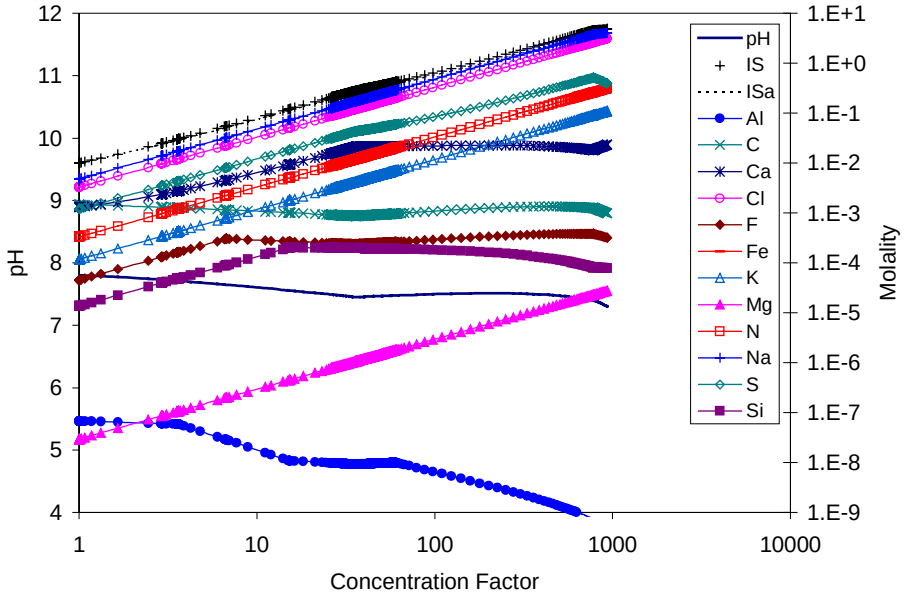

DTN: MO0112MWDHRH10.025

Figure 57. Aqueous Evaporative Evolution of Cement Leachate for the REV 01 THC Model Abstraction at the Crown of the Drift in the Tptpmn Lithology, Period 5

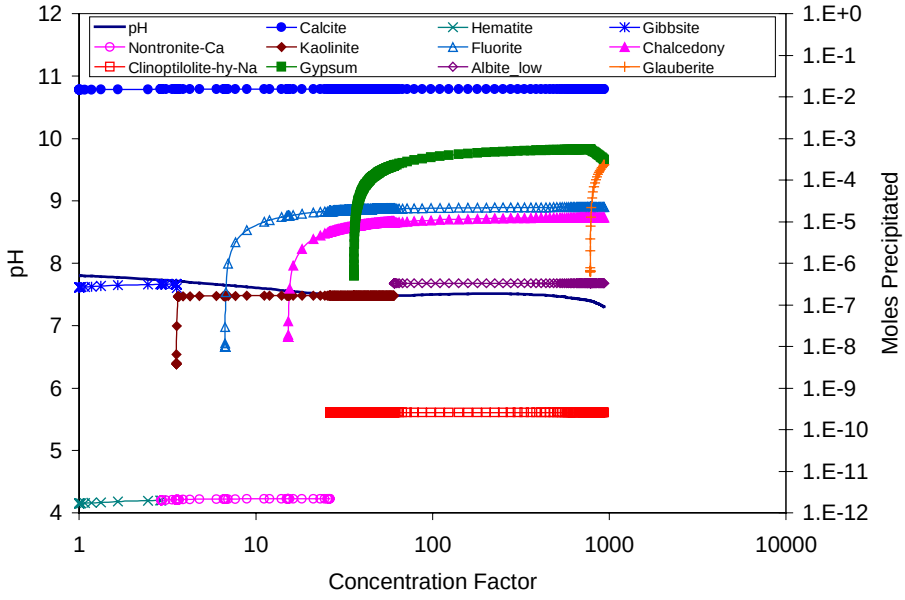

DTN: MO0112MWDHRH10.025

Figure 58. Mineral Evaporative Evolution of Cement Leachate for the REV 01 THC Model Abstraction at the Crown of the Drift in the Tptpmn Lithology, Period 5

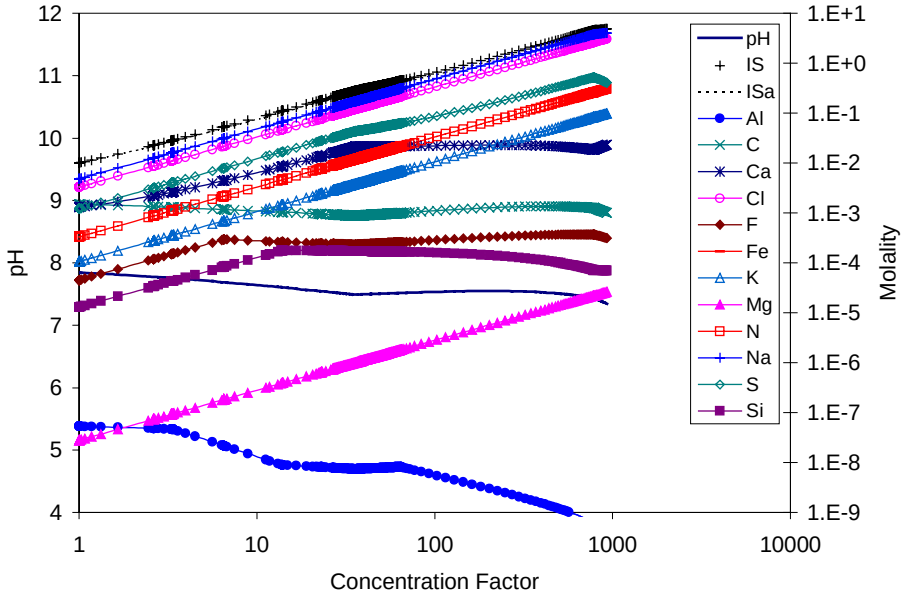

DTN: MO0112MWDHRH10.025

Figure 59. Aqueous Evaporative Evolution of Cement Leachate for the REV 01 THC Model Abstraction at the Crown of the Drift in the Tptpmn Lithology, Period 6

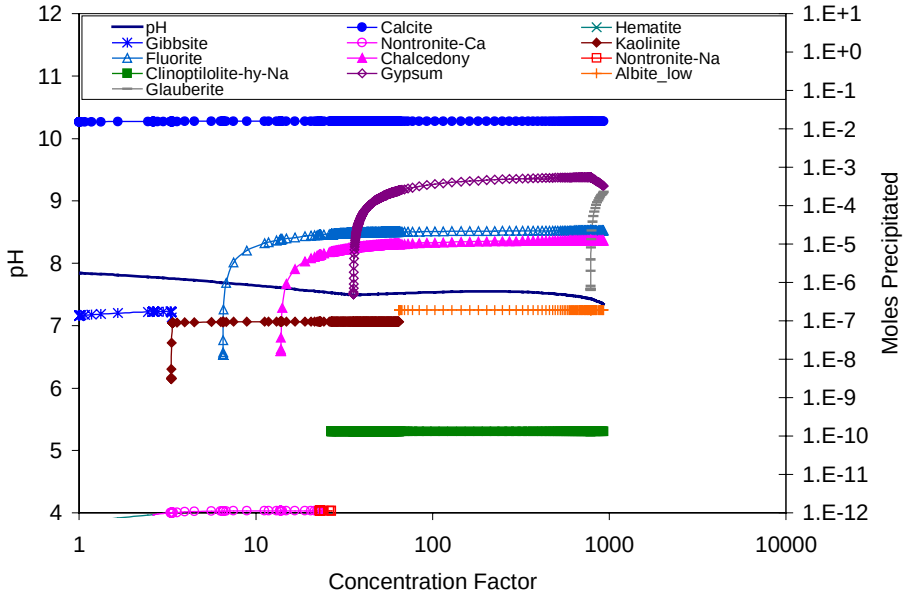

DTN: MO0112MWDHRH10.025

Figure 60. Mineral Evaporative Evolution of Cement Leachate for the REV 01 THC Model Abstraction at the Crown of the Drift in the Tptpmn Lithology, Period 6

6.1.2.9 Different Cement Grout Leachate (Water #9)

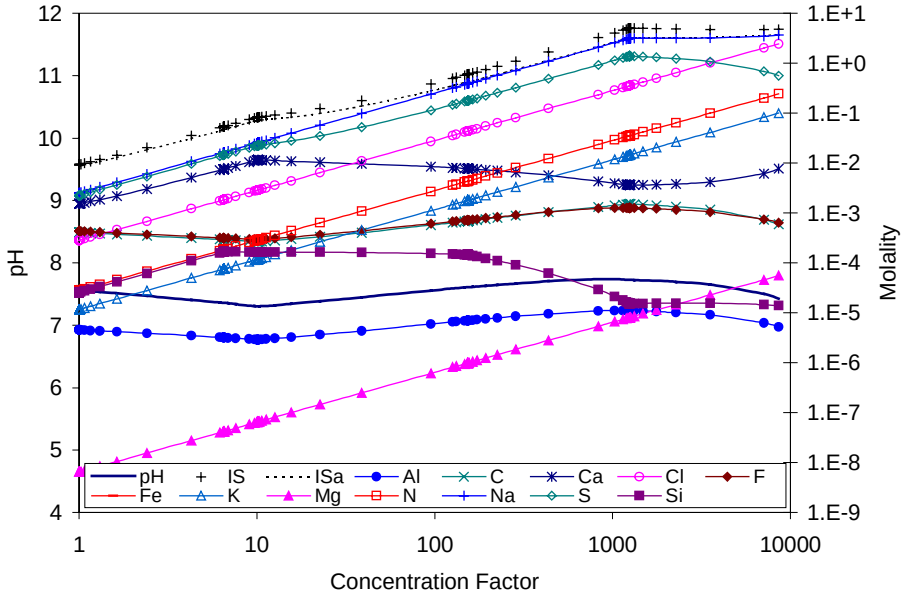

DTN: MO0112MWDHRH10.025

Figure 61. Aqueous Evaporative Evolution of Cement Leachate for the REV 01 THC Model Abstraction (for SSPA) at the Crown of the Drift of the High Temperature and High Carbon Dioxide Partial Pressure Case in the Tptpll Lithology, Initialized Using Water Composition of UZ-14 Perched Water, Period 1

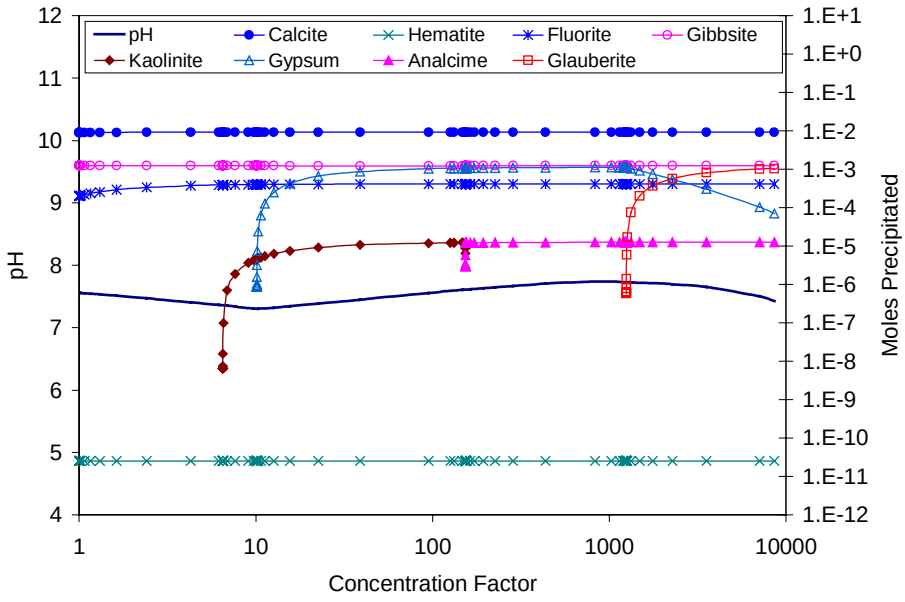

DTN: MO0112MWDHRH10.025

Figure 62. Mineral Evaporative Evolution of Cement Leachate for the REV 01 THC Model Abstraction (for SSPA) at the Crown of the Drift of the High Temperature and High Carbon Dioxide Partial Pressure Case in the Tptpll Lithology, Initialized Using Water Composition of UZ-14 Perched Water, Period 1

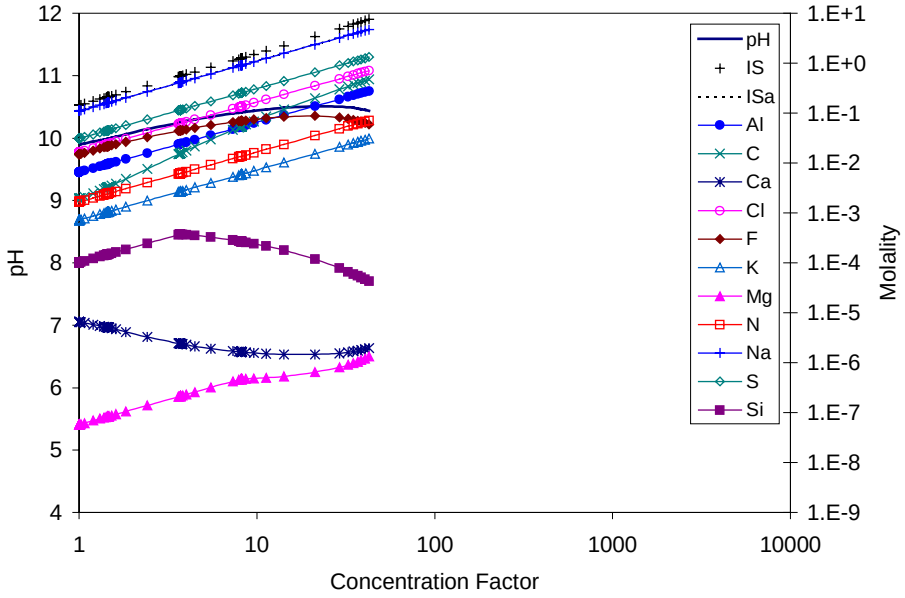

DTN: MO0112MWDHRH10.025

Figure 63. Aqueous Evaporative Evolution of Cement Leachate for the REV 01 THC Model Abstraction (for SSPA) at the Crown of the Drift of the High Temperature and High Carbon Dioxide Partial Pressure Case in the Tptpll Lithology, Initialized Using Water Composition of UZ-14 Perched Water, Period 2

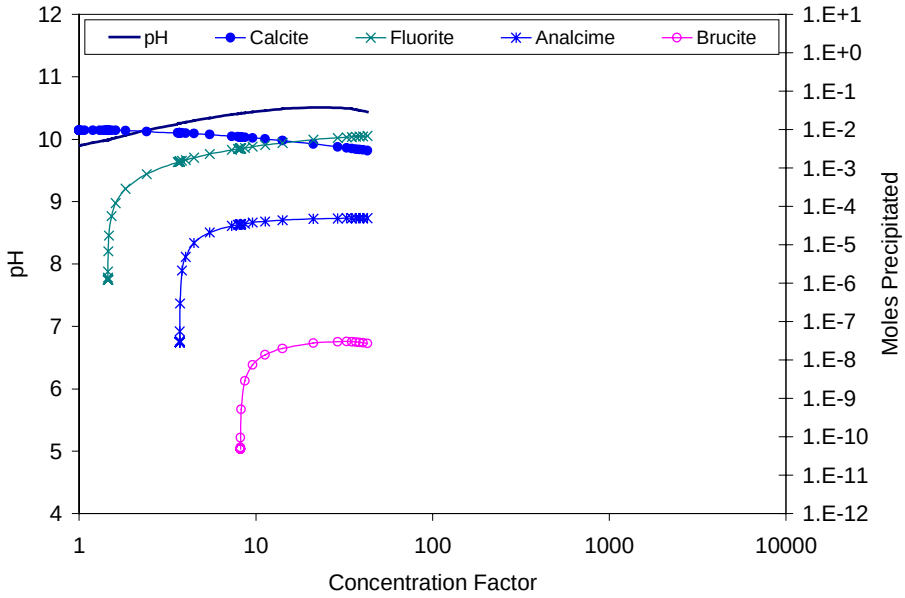

DTN: MO0112MWDHRH10.025

Figure 64. Mineral Evaporative Evolution of Cement Leachate for the REV 01 THC Model Abstraction (for SSPA) at the Crown of the Drift of the High Temperature and High Carbon Dioxide Partial Pressure Case in the Tptpll Lithology, Initialized Using Water Composition of UZ-14 Perched Water, Period 2

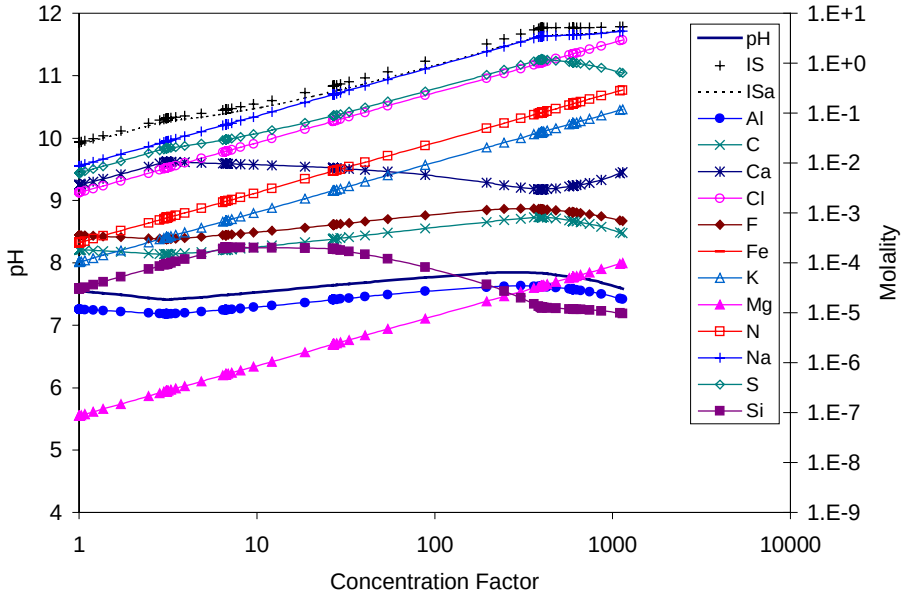

DTN: MO0112MWDHRH10.025

Figure 65. Aqueous Evaporative Evolution of Cement Leachate for the REV 01 THC Model Abstraction (for SSPA) at the Crown of the Drift of the High Temperature and High Carbon Dioxide Partial Pressure Case in the Tptpll Lithology, Initialized Using Water Composition of UZ-14 Perched Water, Period 3

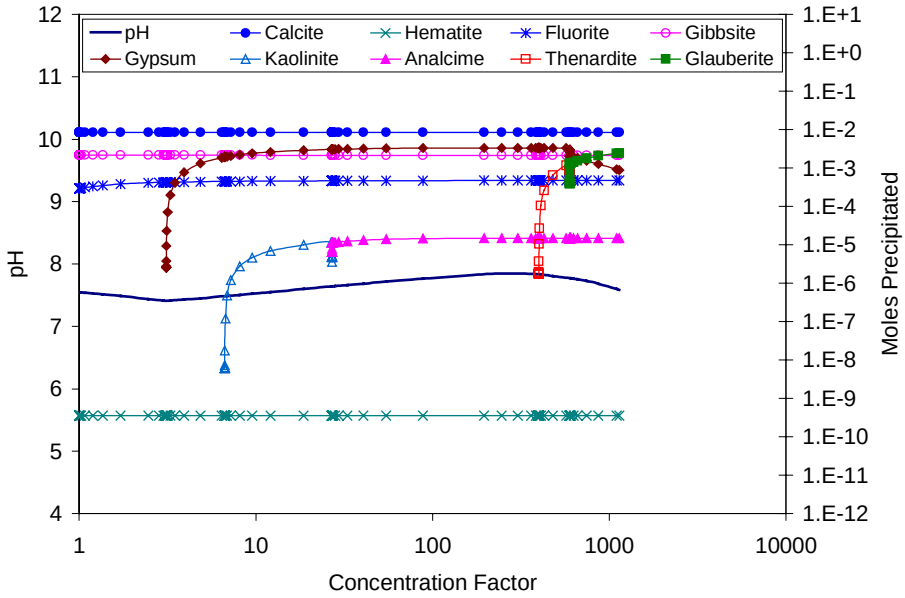

DTN: MO0112MWDHRH10.025

Figure 66. Mineral Evaporative Evolution of Cement Leachate for the REV 01 THC Model Abstraction (for SSPA) at the Crown of the Drift of the High Temperature and High Carbon Dioxide Partial Pressure Case in the Tptpll Lithology, Initialized Using Water Composition of UZ-14 Perched Water, Period 3

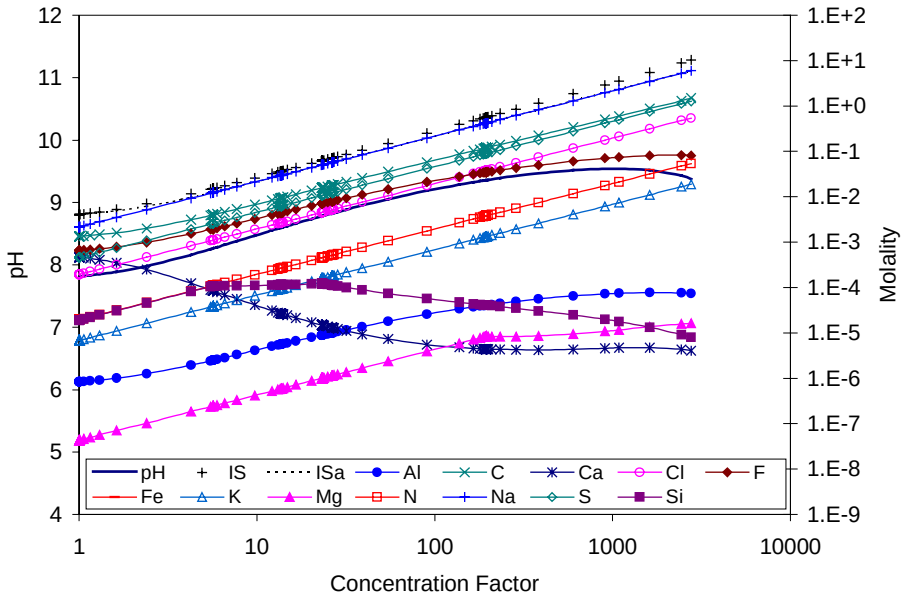

DTN: MO0112MWDHRH10.025

Figure 67. Aqueous Evaporative Evolution of Cement Leachate for the REV 01 THC Model Abstraction (for SSPA) at the Crown of the Drift of the High Temperature and High Carbon Dioxide Partial Pressure Case in the Tptpll Lithology, Initialized Using Water Composition of UZ-14 Perched Water, Period 4

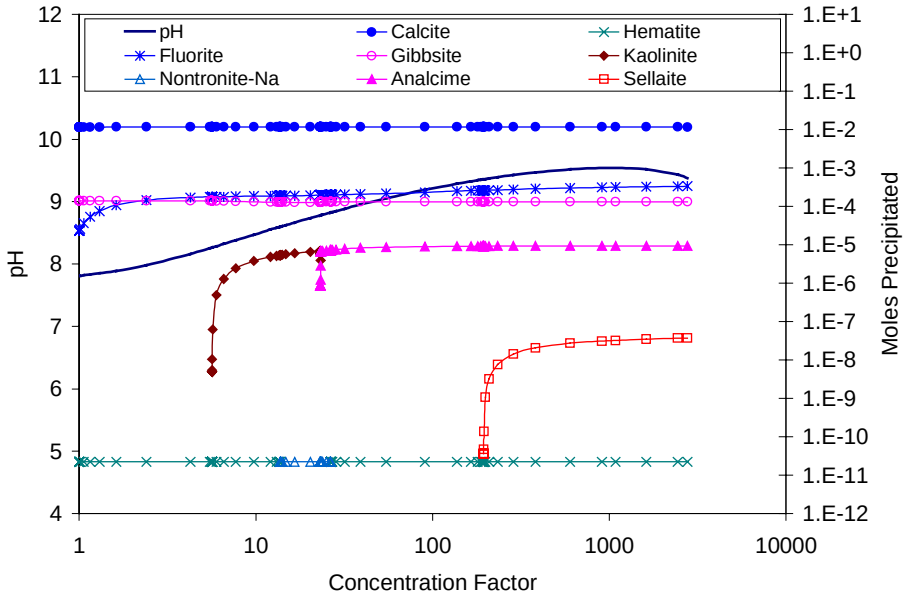

DTN: MO0112MWDHRH10.025

Figure 68. Mineral Evaporative Evolution of Cement Leachate for the REV 01 THC Model Abstraction (for SSPA) at the Crown of the Drift of the High Temperature and High Carbon Dioxide Partial Pressure Case in the Tptpll Lithology, Initialized Using Water Composition of UZ-14 Perched Water, Period 4

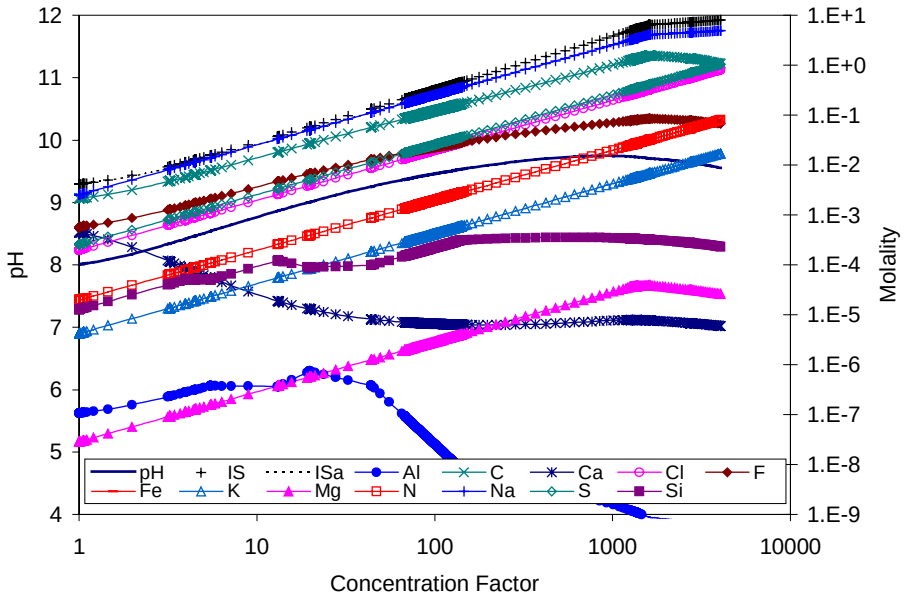

DTN: MO0112MWDHRH10.025

Figure 69. Aqueous Evaporative Evolution of Cement Leachate for the REV 01 THC Model Abstraction (for SSPA) at the Crown of the Drift of the High Temperature and High Carbon Dioxide Partial Pressure Case in the Tptpll Lithology, Initialized Using Water Composition of UZ-14 Perched Water, Period 5

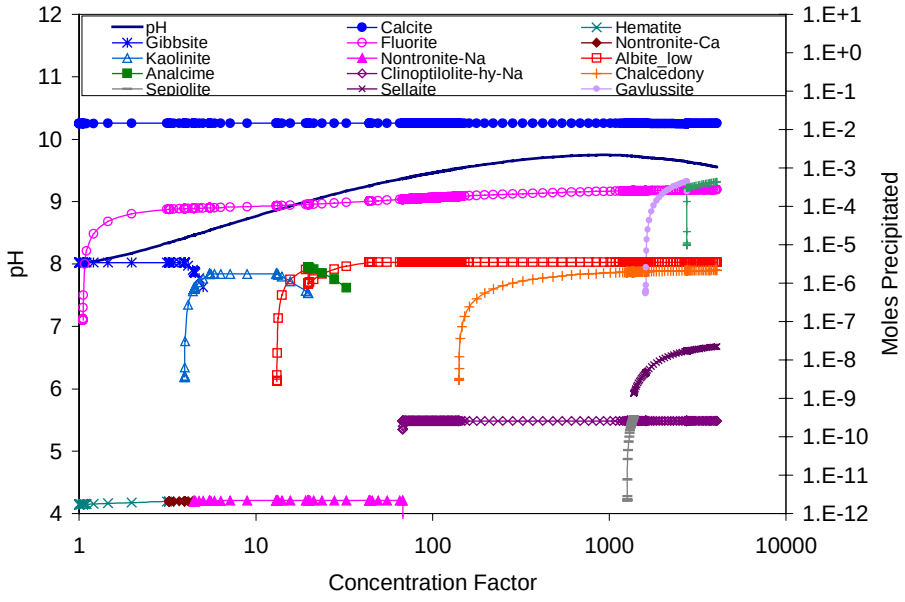

DTN: MO0112MWDHRH10.025

Figure 70. Mineral Evaporative Evolution of Cement Leachate for the REV 01 THC Model Abstraction (for SSPA) at the Crown of the Drift of the High Temperature and High Carbon Dioxide Partial Pressure Case in the Tptpll Lithology, Initialized Using Water Composition of UZ-14 Perched Water, Period 5

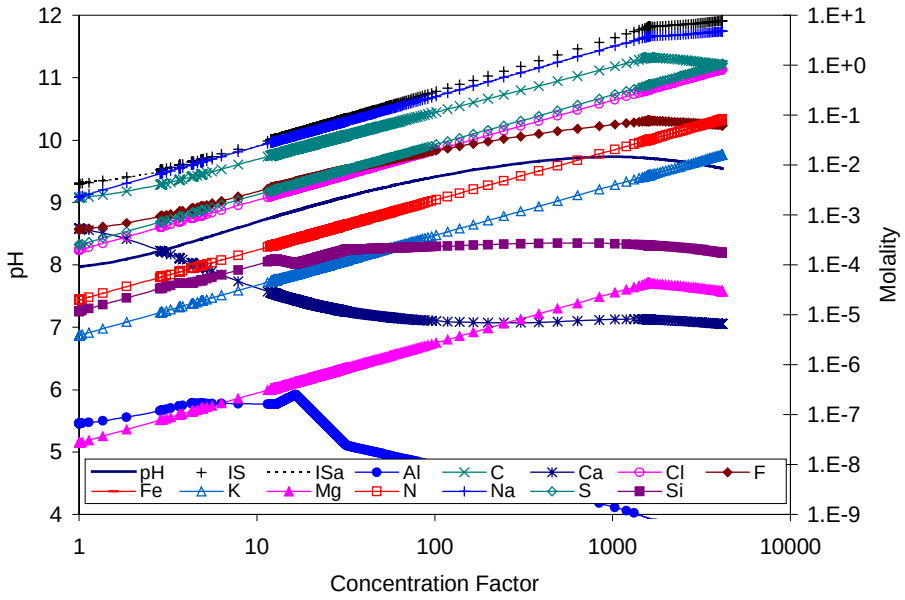

DTN: MO0112MWDHRH10.025

Figure 71. Aqueous Evaporative Evolution of Cement Leachate for the REV 01 THC Model Abstraction (for SSPA) at the Crown of the Drift of the High Temperature and High Carbon Dioxide Partial Pressure Case in the Tptpll Lithology, Initialized Using Water Composition of UZ-14 Perched Water, Period 6

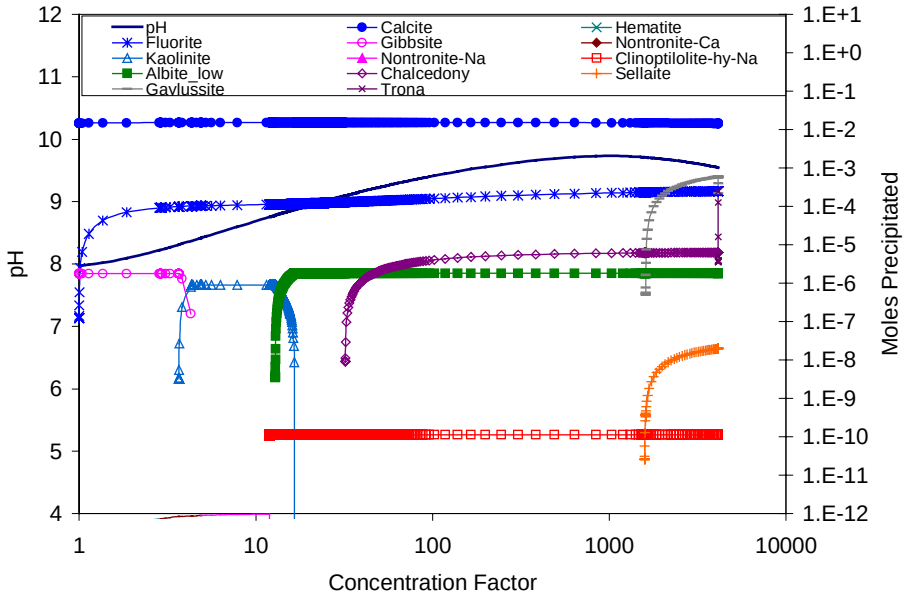

DTN: MO0112MWDHRH10.025

Figure 72. Mineral Evaporative Evolution of Cement Leachate for the REV 01 THC Model Abstraction (for SSPA) at the Crown of the Drift of the High Temperature and High Carbon Dioxide Partial Pressure Case in the Tptpll Lithology, Initialized Using Water Composition of UZ-14 Perched Water, Period 6

6.1.3 Summary of Effects of Starting Water Composition

The evaporation predictions presented in this calculation reveal several important chemical divides for the waters investigated. These chemical divides play a major role in the type of brine that could develop in the potential repository.

The first important chemical divide encountered in most simulations is the calcite chemical divide. The effects of the calcite chemical divide are apparent during the early stages of evaporation because the starting waters are usually either saturated or nearly saturated with respect to calcite.

Figures 1 through 6 show the Precipitates/Salts model prediction of the evaporative evolution of in situ J-13 ground water (water #1 in Table 1) at CO_2 fugacities of 10^{-1}, 10^{-3}, and 10^{-6}. For this water, a carbonate-rich, Ca-poor water evolves similar to that observed in the laboratory for synthetic J-13 well water (Rosenberg et al. 1999a). Perched water (#3) and waters collected from the Single Heater Test (#4) and Drift-Scale Heater Test (#5) give similar results, as shown in Figures 13 through 30. In each of these cases, regardless of the fixed fugacity of CO_2, Na becomes the dominant cation and CO_3 (except for water #5) becomes the dominant anion. For water #5, the Drift-Scale Heater Test water, Cl becomes the dominant anion for the maximum concentration factors simulated.

It is not clear what happens as a result of further evaporation of the Drift-Scale Heater Test water (#5) beyond the range of the HRH model. As evaporation generates higher salinities, the chemical divides for the Na-(K)-Cl-CO_3-SO_4 system will be encountered. CO_3 is highly soluble under highly alkaline conditions (Stumm and Morgan 1996, Figure 4.5). If it is the most soluble of the three anions under these circumstances, then Cl and sulfate (SO_4) would be depleted by the precipitation of halite and sodium sulfate salts, and this water (#5) would also be predicted to generate a sodium carbonate brine.

For Topopah Spring tuff pore water (#2) and predicted REV 00 seepage water (#6), the calcite chemical divide causes depletion of CO_3 and concentration of aqueous Ca. The predicted evaporative evolution of these waters are displayed in Figures 7 through 12 (#2) and 31 through 36 (#6). The reason CO_3 is depleted instead of Ca is that these waters have excess equivalent Ca relative to carbonate alkalinity.

The REV 01 THC abstraction water (#7) and cement leachate predicted to result from contacting this water (#8) show excess equivalent Ca relative to CO_3 (Figures 37 through 60). However, because CO_3 concentrations are very low in these waters, the calcite chemical divide has a limited effect on the depletion or concentration of Ca and CO_3 as the water evaporates. In one case, as shown in Figure 40, calcite does not precipitate at all. In this case and many of the other simulations for waters #7 and #8, gypsum is the predominant control on Ca concentrations.

Evaporation of cement grout leachate for the REV 01 THC abstraction of the high temperature and high carbon dioxide partial pressure case (#9) shows both sides of the calcite chemical divide, depending on the period simulated. For periods 1 and 3, CO_3 concentrations remain low and excess Ca concentrates until the gypsum chemical divide is encountered. In periods 2, 4, 5,

and 6, however, CO_3 concentrations are much higher relative to Ca, resulting in the depletion of Ca concentrations as the water evaporates.

For the waters with high Ca concentrations relative to CO_3 alkalinity, the gypsum ($CaSO_4 \cdot 2H_2O$) chemical divide is usually encountered after the calcite chemical divide (Drever 1988 p. 236). Accordingly, waters #2, #6, #7, #8, and some of #9 follow this pattern. The gypsum chemical divide generally causes either Ca or SO_4 to become depleted, depending on the Ca:SO_4 molar ratio in solution. In waters #6 and #9 and most of waters #7 and #8, there is excess SO_4 compared to Ca, so Ca becomes depleted. For water #2 and period 3 of waters #7 and #8, there is excess Ca, so SO_4 becomes depleted and Ca continues to concentrate in solution. The chemical divides of other Ca minerals, such as fluorite and various Ca (hydroxy)silicates, may be encountered anywhere during the reaction progress, but they do not affect the Ca concentration appreciably unless the concentrations of the non-Ca reactants are within a factor of about 10 of Ca or are greater than Ca.

Another important chemical divide is the halite (NaCl) chemical divide. This divide is encountered beyond the range of the HRH model. For waters in which there is more Na than Cl, Cl will become depleted. For water #2, and period 3 of waters #7 and #8, there is excess Cl, so Na will become depleted. Thus, these are the waters in which a chloride brine is likely to develop.

Other important divides at the approximate salinity of halite precipitation include divides for villiaumite (NaF), sylvite (KCl), fluorite (CaF_2), and sellaite (MgF_2). If there is excess Ca and Cl, as in the case of water #2, a calcium chloride brine will develop because Na and K would be depleted by the precipitation of halite and sylvite. If there is excess Na and K, as in waters #6 and #9, a Na/K nitrate brine will likely develop because the other potential Na and K salts are not as soluble as the nitrate salts (CRWMS M&O 2000c, Table 9). Although the generation of a potassium fluoride/nitrate brine is possible, it does not occur in the waters evaluated because it requires an excess of fluorine (F). The solubilities of salts of the Na-K-Ca-Mg-F-NO_3 system (CRWMS M&O 2000c, Table 9) indicate that an excess of F would deplete Ca, Mg, and Na through precipitation of fluorite, sellaite, and villiaumite. KF and KNO_3 are extremely soluble in comparison (CRWMS M&O 2000c, Figure 8 and Table 9).

Thus, out of the 36 evaporation simulations presented in this report, five (i.e., 14%) are predicted to evolve into a chloride brine: water #2 and period 3 of waters #7 and #8. Water #2 was used to initialize the Topopah Spring tuff matrix and fracture water composition in the THC model for the REV 01 calculations. These results may have important implications for the relative humidity threshold assumption used by TSPA because chloride brines can occur at lower relative humidity than a brine composed largely of sodium nitrate. Overall, the results of the sensitivity calculations indicate that the evaporative evolution of water in the drift is highly sensitive to the incoming seepage water composition.

6.2 EFFECTS OF MINERAL SUPPRESSIONS ON EVAPORATIVE EVOLUTION

In a multi-component hydrogeochemical system, such as pore water in tuff, it is difficult to predict each mineral that would precipitate as a result of evaporation. Precipitation of some minerals may be inhibited by a lack of nucleation sites or by slow kinetics. Often, however, data

needed to determine what would likely happen for potential minerals are either unavailable or inconclusive. In the sensitivity calculations, the sensitivity of mineral suppressions to precipitates/salts model output was assessed by varying the set of suppressed minerals and evaluating the effects on the precipitates/salts model predictions.

The first sensitivity calculation performed on mineral suppressions is documented in Section 5.4 of *In-Drift Precipitates/Salts Analysis* (BSC 2001b). Albite-low was suppressed in one set of calculations and then unsuppressed in an identical set of calculations. The results indicated that while the mineral assemblage changed (albite-low precipitated in one set but not in the other) and the Al concentration was affected, the suppression had no effect on the output (pH, Cl, and ionic strength) to TSPA. Al was a minor constituent in the incoming seepage water and therefore albite-low was a minor constituent of the mineral assemblage. This calculation suggests that minerals that involve minor constituents will not markedly affect Cl and ionic strength predictions. However, it is theoretically possible that suppression of minor constituents may affect pH because the hydrogen ion activity may also be low (e.g., 10^{-8} at pH 8) and poorly buffered.

The addition of several minerals to the PT5v2 Pitzer database provided another opportunity to assess the sensitivity of mineral suppressions. The PT4 Pitzer database was used in the REV 00 TSPA calculations (CRWMS M&O 2001). These original calculations are plotted in more detail in Figures 16 through 21 of Mariner (2001). Of the minerals added to the PT5v2 database, only okenite and gyrolite were allowed to precipitate upon supersaturation. The largest change in the calculations resulted from the precipitation of gyrolite. During the boiling period (period 2) of the REV 00 THC abstraction, precipitation of gyrolite lowered the pH nearly a full unit from around 9.3 to around 8.5 (Figure 17 of Mariner 2001 versus Figure 32 above). However, Cl and ionic strength were essentially unaffected. For periods 3 and 4 the pH, Cl, and ionic strength predictions were unaffected because gyrolite was no longer favored to precipitate.

While the above calculations suggest that the uncertainty in mineral suppressions may have only minor effects on the pH, Cl, and ionic strength outputs to TSPA, more work is warranted to evaluate the uncertainty and sensitivity of mineral suppressions on TSPA calculations.

6.3 EFFECTS OF CO_2 FUGACITY ON EVAPORATIVE EVOLUTION

Evaporation of waters #1 through #5 in Table 1 was simulated at three different CO_2 fugacities: 10^{-1}, 10^{-3}, and 10^{-6}. The results are displayed in Figures 1 through 30.

The CO_2 fugacity has a large effect on pH. In each case, the pH increases 2 to 3 pH units as the CO_2 fugacity decreases from 10^{-1} to 10^{-6}. This is not surprising because CO_2 reacts with water (H_2O) to produce carbonic acid (H_2CO_3) (Drever 1988, p. 48).

The CO_2 fugacity also has a large effect on dissolved CO_3. At early stages of evaporation, the CO_3 concentration is 2 to 3 orders of magnitude lower at a CO_2 fugacity of 10^{-6} than at 10^{-1}. Although the large difference persists at later stages of evaporation for the Topopah Spring tuff pore water (#2), it nearly disappears for the other waters (#1, #3, #4, and #5). The reason appears to be largely due to the differences in pH values. At a CO_2 fugacity of 10^{-6}, water #2 has a pH around 8 at high concentration factors whereas the other waters have pH values around 11

under the same conditions. High pH values increase the equilibrium dissolved CO_3 concentration when the CO_2 fugacity is fixed (Stumm and Morgan 1996, Figure 4.5).

Mineral assemblages often change depending on the CO_2 fugacity. For example, when the fugacity is 10^{-6}, gyrolite (a calcium hydroxysilicate) precipitates. This is likely due in part to the higher pH values at this CO_2 fugacity. Another observation is that trona ($Na_3CO_3HCO_3 \cdot 2H_2O$) begins to precipitate within the range of the HRH model for the Single Heater Test sample (#4) when the CO_2 fugacity is 10^{-1} (Figure 20). If the model is accurate, it suggests that the lower pH values caused by the increased CO_2 fugacity, combined with the high concentrations of Na and CO_3 relative to other dissolved solids at high concentration factors, allow trona to precipitate at ionic strengths within the range of the HRH model. Trona might actually precipitate at lower CO_2 fugacities and for waters #1, #3, and #5, but if so, it would require concentration factors higher than allowed by the HRH model.

Cl concentrations are essentially unaffected by the CO_2 fugacity. Cl does not precipitate in any of the evaporation simulations within the range of the HRH model.

Unlike Cl, ionic strength is noticeably affected by CO_2 fugacity. The effects are most apparent at the earliest and latest stages of evaporation. At the early stages, Ca contributions to ionic strength are important. However, for waters #1, #3, #4, and #5, Ca becomes depleted by mineral precipitation before evaporation raises the concentration factor to about 10. Once Ca begins to precipitate, Ca contributions to ionic strength become negligible and a change of slope is observed for the ionic strength. As shown in the figures, the changes in ionic strength at low concentration factors are slightly affected by the CO_2 fugacity. The CO_2 fugacity affects both pH and CO_3 concentrations, which in turn affect Ca concentrations.

At high ionic strength, CO_2 fugacity generally has little effect in the range of the HRH model. The major exception is the evaporation of the Single Heater Test water at a CO_2 fugacity of 10^{-1} when trona is predicted to begin precipitating (Figure 19). This is the only case in which the dominant cation and anion begin exclusively precipitating.

For the Topopah Spring tuff pore water (#2) evaporation, the effects of CO_2 fugacity on ionic strength are negligible. In this water, Ca concentrations are not controlled by the carbonate system because there is a large excess of Ca relative to CO_3. Instead, Ca concentrations are largely controlled by the SO_4 concentration by the precipitation of gypsum at concentration factors greater than 10. SO_4 concentrations do not change in these simulations as the CO_2 fugacity changes.

As for the effects of CO_2 fugacity on the overall type of brine that develops in these simulations, they are minimal for these waters. In each case, the dominant ions at the highest concentration factors simulated do not change as a result of varying the CO_2 fugacity. However, the relative concentrations of these ions do change slightly. As discussed in Section 6.1.3, these small changes may have important effects when chemical divides are encountered beyond the range of the HRH model.

6.4 UNCERTAINTY AND LIMITATIONS

The model results for each water composition evaluated in this calculation are designated as qualified technical product output (TPO) for the purposes of sensitivity analysis. The output DTNs produced or compared in this calculation are listed in Section 7.2.2 and Table 2. Five of the waters (#1, #2, #6, #8, and #9 in Table 1) use data from qualified DTNs as input. Their results are documented in DTN: MO0112MWDHRH10.025. Three of the waters (#3, #4, and #5 in Table 1) do not use data from qualified DTNs. Instead, they are qualified for use in the sensitivity calculations using assumptions and corroborative data. The results for these three waters are documented in DTN: MO0112MWDHRH10.026. Output for water #7 is qualified TPO developed in *Precipitates/Salts Model Calculations For Various Drift Temperature Environments* (BSC 2001c, DTN: MO0112MWDTHC12.024). The uncertainty and limitations of the high relative humidity salts submodel used to produce the results in this calculation are summarized in Section 7.3 of the *In-Drift Precipitates/Salts Analysis* (BSC 2001b).

7. REFERENCES

7.1 DOCUMENTS

BSC (Bechtel SAIC Company) 2001a. *Technical Work Plan For Engineered Barrier System Department Modeling and Testing FY 02 Work Activities*. TWP-MGR-MD-000015 Rev 01. Las Vegas, Nevada: Bechtel SAIC Company. URN-0993

BSC 2001b. *In-Drift Precipitates/Salts Analysis*. ANL-EBS-MD-000045 REV 00 ICN 03. Las Vegas, Nevada: Bechtel SAIC Company. URN-0957

BSC 2001c. *Precipitates/Salts Model Calculations For Various Drift Temperature Environments*. CAL-EBS-PA-000012 REV 00. Las Vegas, Nevada: Bechtel SAIC Company. URN-0956

BSC 2001d. *EBS Incoming Water and Gas Composition Abstraction Calculations for Different Drift Temperature Environments*. CAL-EBS-PA-000013 REV 00. Las Vegas, Nevada: Bechtel SAIC Company. Submit to RPC URN-0960

CRWMS M&O 1997. *Single Heater Test Status Report.* BAB000000-01717-5700-00002 REV 01. Las Vegas, Nevada: CRWMS M&O. ACC: MOL.19980416.0696.

CRWMS M&O 1998b. "Near-Field Geochemical Environment." Chapter 4 of *Total System Performance Assessment-Viability Assessment (TSPA-VA) Analyses Technical Basis Document.* B00000000-01717-4301-00004 REV 01. Las Vegas, Nevada: CRWMS M&O. ACC: MOL.19981008.0004.

CRWMS M&O 1999b. *Addendum to: EQ6 Computer Program for Theoretical Manual, Users Guide, & Related Documentation*. Software Change Request LSCR198. Las Vegas, Nevada: CRWMS M&O. ACC: MOL.19990305.0112.

CRWMS M&O 2000a. *Analysis of Geochemical Data for the Unsaturated Zone*. ANL-NBS-HS-000017 REV 00. Las Vegas, Nevada: CRWMS M&O. ACC: MOL.20000725.0453.

CRWMS M&O 2000b. *Total System Performance Assessment for the Site Recommendation.* TDR-WIS-PA-000001 REV 00 ICN 01. Las Vegas, Nevada: CRWMS M&O. ACC: MOL.20001220.0045.

CRWMS M&O 2000c. *Environment on the Surfaces of the Drip Shield and Waste Package Outer Barrier*. ANL-EBS-MD-000001 REV 00 ICN 01. Las Vegas, Nevada: CRWMS M&O. ACC: MOL.20001219.0080.

CRWMS M&O 2001. *Precipitates/Salts Model Results for THC Abstraction.* CAL-EBS-PA-000008 REV 00 ICN 01. Las Vegas, Nevada: CRWMS M&O. ACC: MOL.20010125.0231.

Drever, J.I. 1988. *The Geochemistry of Natural Waters.* 2nd Edition. Englewood Cliffs, New Jersey: Prentice-Hall. TIC: 242836.

Eugster, H.P. and Hardie, L.A. [1978]. "Saline Lakes." *Lakes, Chemistry, Geology, Physics*. Lerman, A., ed. Pages 237-293. New York, New York: Springer-Verlag. TIC: 240782.

Eugster, H.P. and Jones, B.F. 1979. "Behavior of Major Solutes During Closed-Basin Brine Evolution." *American Journal of Science*, 279, 609-631. New Haven, Connecticut: Yale University, Kline Geology Laboratory. TIC: 234258.

Garrels, R.M. and Mackenzie, F.T. 1967. "Origin of the Chemical Compositions of Some Springs and Lakes?." *Equilibrium Concepts in Natural Water Systems*. American Chemical Society Advances in Chemistry Series 67. Pages 222-242. Washington, D.C.: American Chemical Society. TIC: 246519.

Harrar, J.E.; Carley, J.F.; Isherwood, W.F.; and Raber, E. 1990. *Report of the Committee to Review the Use of J-13 Well Water in Nevada Nuclear Waste Storage Investigations*. UCID-21867. Livermore, California: Lawrence Livermore National Laboratory. ACC: NNA.19910131.0274.

Klein, C. and Hurlbut, C.S., Jr. 1999. *Manual of Mineralogy*. 21st Edition, Revised. New York, New York: John Wiley & Sons. TIC: 246258.

Mariner, P. 2001. "Informal Calculation Regarding Precipitates/Salts Model Sensitivity Analyses in Support of SSPA Volume 1." Memorandum from P. Mariner (BSC) to B. MacKinnon, May 30, 2001, PROJ.05/01.075, with enclosure. ACC: MOL.20010531.0029.

Rosenberg, N.D.; Knauss, K.G.; and Dibley, M.J. 1999a. *Evaporation of J13 Water: Laboratory Experiments and Geochemical Modeling*. UCRL-ID-134852. Livermore, California: Lawrence Livermore National Laboratory. TIC: 246322.

Rosenberg, N.D.; Knauss, K.G.; and Dibley, M.J. 1999b. *Evaporation of Topopah Spring Tuff Pore Water*. UCRL-ID-135765. [Livermore, California]: Lawrence Livermore National Laboratory. TIC: 246231.

Stumm, W. and Morgan, J.J. 1996. *Aquatic Chemistry, Chemical Equilibria and Rates in Natural Waters*. 3rd Edition. New York, New York: John Wiley & Sons. TIC: 246296.

Wolery, T.J. 1992a. EQ3/6, *A Software Package for Geochemical Modeling of Aqueous Systems: Package Overview and Installation Guide (Version 7.0).* UCRL-MA-110662 PT I. Livermore, California: Lawrence Livermore National Laboratory. TIC: 205087.

Wolery, T.J. 1992b. *EQ3NR, A Computer Program for Geochemical Aqueous Speciation-Solubility Calculations: Theoretical Manual, User's Guide, and Related Documentation (Version 7.0)*. UCRL-MA-110662 PT III. Livermore, California: Lawrence Livermore National Laboratory. ACC: MOL.19980717.0626.

Wolery, T.J. and Daveler, S.A. 1992. *Theoretical Manual, User's Guide, and Related Documentation, Version 7.0*. Volume IV of EQ6, A Computer Program for Reaction Path Modeling of Aqueous Geochemical Systems. UCRL-MA-110662. Draft 1.1. Livermore, California: Lawrence Livermore National Laboratory. TIC: 238011.

7.2 DATA, LISTED BY TRACKING NUMBER

7.2.1 Input Data and Corroborative Data

LB0101DSTTHCR1.001. Pore Water Composition and CO2 Partial Pressure Input to Thermal-Hydrological-Chemical (THC) Simulations: Table 3 of AMR N0120/U0110 Rev01, "Drift-Scale Coupled Processes (Drift-Scale Heater Test and THC Seepage) Models". Submittal date: 01/26/2001.

LL970409604244.030. Second Quarter Results of Chemical Measurements in the Single Heater Test. Submittal date: 04/17/1997.

LL990702804244.100. Borehole and Pore Water Data. Submittal date: 07/13/1999.

MO0006J13WTRCM.000. Recommended Mean Values of Major Constituents in J-13 Well Water. Submittal date: 06/07/2000.

MO0110SPAEBS13.038. EBS Incoming Water and Gas Composition Abstraction Calculation Results. Submittal date: 10/16/2001. URN-0968

MO0112MWDTHC12.024. High Relative Humidity Salts Model Predictions for THC REV 01 Using PT5v2 Thermodynamic Database. Submittal date: 11/28/2001. URN-0996

MO9912SPAPAI29.002. PA Initial Abstraction of THC Model Chemical Boundary Conditions. Submittal date: 01/11/2000.

MO0111SPATHC14.040. Seepage Grout Interactions Calculations for THC Seepage Waters. Submittal date: 11/21/01. URN-0995

MO0110SPAPT245.017. PT5 Pitzer Database for EQ3/6, Version 2. Submittal date: 10/04/2001. URN-0994

7.2.2 Developed Data

MO0112MWDHRH10.025. High Relative Humidity Salts Model Predictions for Sensitivity Calculations for Waters 1, 2, 6, 8 and 9. Submittal date: 12/12/2001.

MO0112MWDHRH10.026. High Relative Humidity Salts Model Predictions for Sensitivity Calculations for Waters 3, 4, and 5. Submittal date: 12/12/2001.

7.3 CODES, STANDARDS, REGULATIONS, PROCEDURES, AND SOFTWARE

AP-3.12Q, Revision 0, ICN 4. *Calculations.* Washington, D.C.: U.S. Department of Energy, Office of Civilian Radioactive Waste Management. ACC: MOL.20010404.0008.

AP-SI.1Q, Rev. 3, ICN 2, ECN 1. *Software Management*. Washington, D.C.: U.S. Department of Energy, Office of Civilian Radioactive Waste Management. ACC: MOL.20011030.0598.

CRWMS M&O 1998a. *Software Code: EQ3/6*. V7.2b. LLNL: UCRL-MA-110662.

CRWMS M&O 1999a. *Software Code: EQ6, Version 7.2bLV*. V7.2bLV. 10075-7.2bLV-00.